Discovery of bactericides as an acute mitochondrial membrane damage inducer

Ryan Houston[a], Yusuke Sekine[a,b], Mads B Larsen[a], Kei Murakami[c], Steven J. Mullett[d], Stacy G. Wendell[d], Derek P. Narendra[e], Bill B. Chen[a,f,g], and Shiori Sekine[a,h,*]

[a]Aging Institute, Department of Medicine, School of Medicine, University of Pittsburgh, Pittsburgh, PA 15219; [b]Division of Endocrinology and Metabolism, Department of Medicine, School of Medicine, University of Pittsburgh, Pittsburgh, PA 15219; [c]Department of Chemistry, School of Science, Kwansei Gakuin University, Sanda, Hyogo, Japan; [d]Department of Pharmacology and Chemical Biology, the Health Sciences Metabolomics and Lipidomics Core, University of Pittsburgh, Pittsburgh, PA 15261; [e]Inherited Movement Disorders Unit, Neurogenetics Branch, National Institute of Neurological Disorders and Stroke, National Institutes of Health, Bethesda, MD 20892; [f]Acute Lung Injury Center of Excellence, Division of Pulmonary, Allergy, and Critical Care Medicine, Department of Medicine, School of Medicine, University of Pittsburgh, Pittsburgh, PA 15213; [g]Vascular Medicine Institute, Department of Medicine, School of Medicine, University of Pittsburgh, Pittsburgh, PA 15261; [h]Division of Cardiology, Department of Medicine, School of Medicine, University of Pittsburgh, Pittsburgh, PA 15261

ABSTRACT Mitochondria evolved from endosymbiotic bacteria to become essential organelles of eukaryotic cells. The unique lipid composition and structure of mitochondrial membranes are critical for the proper functioning of mitochondria. However, stress responses that help maintain the mitochondrial membrane integrity are not well understood. One reason for this lack of insight is the absence of efficient tools to specifically damage mitochondrial membranes. Here, through a compound screen, we found that two bis-biguanide compounds, chlorhexidine and alexidine, modified the activity of the inner mitochondrial membrane (IMM)-resident protease OMA1 by altering the integrity of the IMM. These compounds are well-known bactericides whose mechanism of action has centered on their damage-inducing activity on bacterial membranes. We found alexidine binds to the IMM likely through the electrostatic interaction driven by the membrane potential as well as an affinity for anionic phospholipids. Electron microscopic analysis revealed that alexidine severely perturbated the cristae structure. Notably, alexidine evoked a specific transcriptional/proteostasis signature that was not induced by other typical mitochondrial stressors, highlighting the unique property of alexidine as a novel mitochondrial membrane stressor. Our findings provide a chemical-biological tool that should enable the delineation of mitochondrial stress-signaling pathways required to maintain the mitochondrial membrane homeostasis.

INTRODUCTION

Mitochondria are essential and multifunctional organelles of the cell that are involved in energy production, metabolic processes, and cellular signaling. Evolutionarily, mitochondria evolved from α-proteobacteria that invaded into host eukaryotic cells. Mitochondria are surrounded by two membranes: the outer mitochondrial membrane (OMM) and the inner mitochondrial membrane (IMM). Both membranes have a characteristic phospholipid composition and structure. Reflecting the endosymbiotic origin of mitochondria, the IMM shares similarity with the lipid composition of bacterial membranes including high levels of cardiolipin (CL) (Horvath and Daum, 2013; Tamura *et al.*, 2020; Tatsuta and Langer, 2017). CL is a nonbilayer forming phospholipid that destabilizes the lipid order in bilayers and induces high membrane curvature. Together with phosphatidylethanolamine (PE), which has similar biophysical properties as CL, these nonbilayer lipids make up approximately ~50% of the phospholipids in the IMM and are more abundant in this membrane than in any other cellular membranes (Horvath and Daum, 2013; Tatsuta and Langer, 2017; Tamura *et al.*, 2020). CL and PE contribute to the characteristic highly folded structure of the IMM as represented by cristae, the concave membrane structure of the IMM (Cogliati *et al.*, 2016). Among the biological membranes in the cells, the IMM is known to possess the highest protein density, allowing various essential bioenergetic reactions to occur. The activities of the IMM-embedded enzymes, including the OXPHOS proteins, rely on the defined lipid composition and structures of the IMM (Cogliati *et al.*, 2016). Therefore, the integrity of the IMM must be carefully monitored and maintained in the face of internal or external insults.

Various mitochondrial stress responses that maintain healthy mitochondrial network have been discovered (Youle, 2019). These include mitophagy, an autophagic degradation of damaged mitochondria (Youle and Narendra, 2011), as well as the mitochondrial unfolded protein response (mtUPR) (Anderson and Haynes, 2020), that up-regulates a specific transcriptional program to relieve mitochondrial proteotoxic stress. Importantly, the existence of small molecules that can mimic a distinct type of mitochondrial damage has significantly contributed to the discovery and understanding of these crucial mitochondrial stress-signaling pathways. For example, the mitochondrial protonophore, carbonyl cyanide m-chlorophenyl hydrazone (CCCP) and the combination of OXPHOS inhibitors, antimycin and oligomycin, have been widely used for the mechanistic analysis of PTEN-induced kinase 1 (PINK1)/Parkin-mediated mitophagy (Narendra *et al.*, 2008; Matsuda *et al.*, 2010; Lazarou *et al.*, 2015). The treatment of the cells with these compounds results in mitochondrial membrane potential loss, one of the hallmarks of OXPHOS dysfunction, triggering mitophagy. In mammalian cells, the mtUPR can be induced by CDDO, an inhibitor of the matrix-resident protease LONP, or GTPP1, a mitochondrial HSP90 inhibitor (Munch and Harper, 2016). Moreover, mitochondrial proteotoxic stress can be induced by actinonin (Richter *et al.*, 2015; Burman *et al.*, 2017), an inducer of mito-ribosome stalling that results in the blockade of mitochondrial protein translation. A series of mitochondrial import blockers, so-called MitoBloCKs, can impair mitochondrial protein import pathways (Hasson *et al.*, 2010; Dabir *et al.*, 2013). Recent omics analyses of the mammalian cells that were treated with these mitochondrial stressors revealed that many of these stressors commonly activate the integrated stress response (ISR) (Quiros *et al.*, 2017). The ISR induces the expression of particular cytoprotective genes through the activation of the transcription factor (ATF4), suggesting the existence of an intimate mitochondria-nuclear communication to activate the proper stress response following specific mitochondrial stressors. Recent studies using cell genetic screens for genes involved in the mitochondrial stressor-induced ISR revealed that mitochondrial proteolysis plays a critical role in activating the ISR (Fessler *et al.*, 2020; Guo *et al.*, 2020). These examples clearly highlight the importance of chemical compounds that can induce a specific mitochondrial stress in identifying and analyzing mitochondrial stress-signaling pathways.

Recent identification of sets of lipid synthesis enzymes and lipid transfer proteins significantly advanced our understanding of lipid metabolism within mitochondria (Tatsuta and Langer, 2017; Tamura *et al.*, 2020). However, it is still not known how mitochondrial membrane homeostasis is preserved under conditions that disturb mitochondrial membrane integrity. This is partly due to a lack of established compounds that can specifically perturb the phospholipid environment of mitochondrial membranes.

Here, through our unbiased small-compound screen that targeted the IMM-integral protease OMA1, we found that two small compounds, chlorhexidine and alexidine, acutely disrupted the integrity of mitochondrial membranes and thereby secondarily alter OMA1 activity. Interestingly, these compounds are known as bactericides that have damage-inducing activities on bacterial membranes. Our biochemical analyses revealed that alexidine had an affinity to mitochondrial membranes and particularly damage the cristae membranes in the IMM. Moreover, we found that the alexidine treatment induced transcriptional and proteostatic signatures that were not observed with other typical mitochondrial stressors. Our discovery therefore provides a unique chemical-biological tool that can acutely and selectively perturb membrane homeostasis in the IMM.

RESULTS

Compound screen of OMA1 inhibitors identifies bactericides

In heathy mitochondria which maintain mitochondrial membrane potential, PINK1 is cleaved by the IMM-resident protease PARL just after the mitochondrial import of PINK1 (Jin *et al.*, 2010) (Supplemental Figure S1A, left panel). The cleaved product of PINK1 is retro-translocated into the cytosol for proteasomal degradation (Yamano and Youle, 2013). In contrast, mitochondrial depolarization induces the mitochondrial import arrest of PINK1, which results in the accumulation of the full-length form of PINK1 and its kinase activation on the OMM of damaged mitochondria (Matsuda *et al.*, 2010; Narendra *et al.*, 2010; Okatsu *et al.*, 2012) (Supplemental Figure S1A, middle panel). Activated PINK1 promotes the autophagic elimination of damaged mitochondria, so-called mitophagy, cooperatively working with the cytosolic E3 ligase Parkin (Youle and Narendra, 2011). Mutations in PINK1 or Parkin cause recessive early onset Parkinson's disease (PD), suggesting a protective role of mitophagy in PD pathogenesis (Youle and Narendra, 2011). We have previously reported that several PD-related PINK1 mutants are insensitive to the mitochondrial stress-dependent import arrest and fail to accumulate in the OMM (Sekine *et al.*, 2019, Sekine, 2020). While these PINK1 mutants are cleaved by PARL in a similar way to PINK1 wild type (WT) in healthy mitochondria, the missorted PINK1 mutants in depolarized mitochondria are instead cleaved by another IMM protease OMA1 and are subsequently subjected to proteasomal degradation (Supplemental Figure S1A, right panel) (Sekine *et al.*, 2019, Sekine, 2020). PINK1 (C125G) is one of these import arrest-defective PD-related PINK1 mutants. We stably expressed PINK1 (C125G)-EYFP in PINK1 knockout (KO) cells and confirmed our previous findings by immunoblotting (IB). PINK1 protein was not observed under steady-state conditions (Figure 1A, lanes 1 and 4). Treatment with the proteasome inhibitor MG132, however, resulted in the accumulation of the cleaved form of PINK1 (C125G)-EYFP (Figure 1A, lanes 3
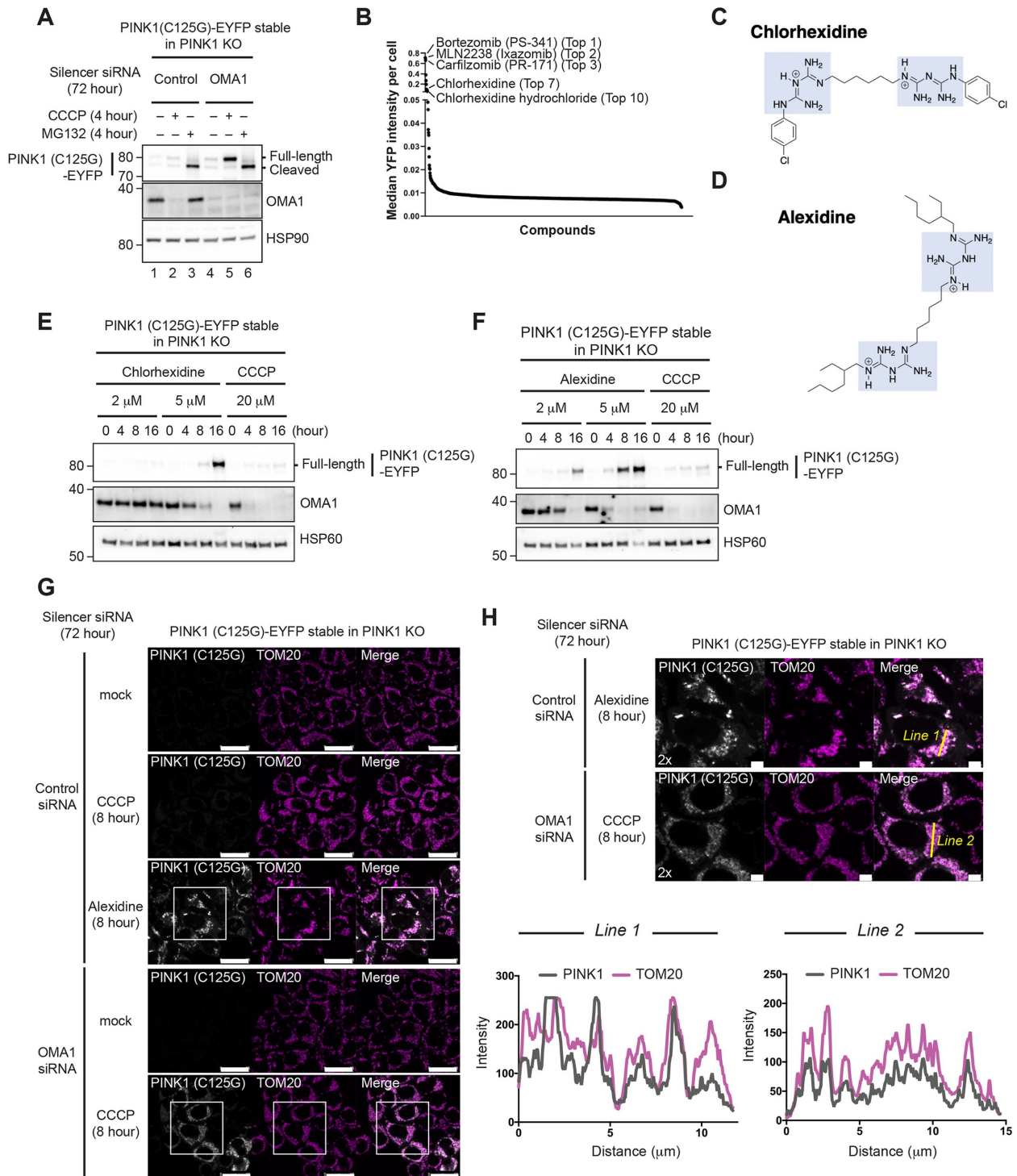
FIGURE 1: Identification of bactericides as a stabilizer of PD-related PINK1 (C125G) mutant. (A) PINK1 KO HeLa cells stably expressed PINK1 (C125G)-EYFP were transfected with control or OMA1 siRNA. After 72 h, cells were treated with 20 μM CCCP or 10 μM MG132 for 4 h. The lysate was analyzed by SDS–PAGE. Note that OMA1 is known to be degraded on CCCP through autocatalytic activation (see also Supplemental Figure S1B). (B) PINK1 KO HeLa cells stably expressed PINK1 (C125G)-EYFP were seeded on 384 well plate and treated with each compound (5 μM, FDA-approved compounds). After 18 h, cells were treated with 20 μM CCCP for 4 h. EYFP fluorescence intensity of each well was measured by the high content image analyzer. (C, D) The chemical structure of a hit compound, chlorhexidine (C), and a similar compound, alexidine (D). Guanidium groups that have delocalized positive charges are highlighted in blue. (E, F) PINK1 KO HeLa cells stably expressed PINK1 (C125G)-EYFP were treated with the indicated drugs for the indicate time period, and the lysate was analyzed by SDS–PAGE. (G, H) HeLa cells stably expressed PINK1 (C125G)-EYFP were transfected with control or OMA1 siRNA. After 72 h, cells were treated with 20 μM CCCP or 5 μM alexidine for 8 h and subjected to ICC. High-magnification images in the indicated regions (G) are shown in H. TOM20 was utilized as a mitochondrial marker. Scale bars; 25 μm (G) and 5 μm (H).

and 6), indicating constitutive proteasomal degradation of PINK1 (C125G)-EYFP after PARL-mediated cleavage in healthy mitochondria. Importantly, PINK1 (C125G)-EYFP could not accumulate in response to CCCP in control siRNA-treated cells (Figure 1A, lane 2), while the full-length form of PINK1 (C125G)-EYFP did accumulate when OMA1 expression was suppressed by an OMA1-specific siRNA (Figure 1A, lane 5). This observation was confirmed by an independent OMA1 siRNA that targets different regions of OMA1 mRNA (Supplemental Figure S1B). Thus, in depolarized mitochondria, PINK1 (C125G)-EYFP is degraded through OMA1.

We realized this assay system might allow for the discovery of OMA1 inhibitors since the level of PINK1 (C125G)-EYFP under depolarized conditions was dependent on OMA1 activity. We, therefore, next measured the intensity of the YFP signal of PINK1 (C125G)-EYFP after CCCP treatment using a high-content image analyzer. The Z′-factor (a factor that can evaluate the effectiveness of a high-throughput screening) calculated by the YFP signal intensity derived from negative control siRNA versus OMA1 siRNA yielded a significantly high value (Z′-factor = 0.74) (Supplemental Figure S1C), indicating the potential robustness of our screening system (Z′ < 0.0, not a suitable assay; 0.0 < Z′ < 0.5, a marginal assay; 0.5 < Z′ < 1.0, an excellent assay; Z′ = 1.0, an ideal assay) (Zhang et al., 1999). The initial screen was performed with an FDA-approved library consisting of approximately 1100 compounds (Supplemental Table S1). The top three hit compounds that induced the accumulation of PINK1 (C125G)-EYFP were proteasome inhibitors (Figure 1B and Supplemental Table S1), confirming that the degradation of PINK1 (C125G)-EYFP occurs through proteasome. Among several other hit compounds, we focused on chlorhexidine and chlorhexidine hydrochloride, which were independently identified within top 10 hits (Figure 1B and Supplemental Table S1). Chlorhexidine is a bis-biguanide compound (Figure 1C) that is clinically used as a bactericide, particularly in hand washing and oral care products (McDonnell and Russell, 1999; Cieplik et al., 2019). There is a similar bis-biguanide compound called alexidine (Figure 1D) (McDonnell and Russell, 1999). These compounds share structural similarities in that they contain symmetrical biguanide units tethered by a long alkyl chain. Strikingly, the treatment with chlorhexidine or alexidine, but not CCCP, significantly promoted PINK1 (C125G) accumulation in a dose- and time-dependent manner (Figure 1, E and F). While both chlorhexidine and alexidine lowered the mitochondrial membrane potential similar to CCCP (Supplemental Figure S1D), these observations suggest a membrane depolarization-independent mechanism for the PINK1 (C125G) accumulation by these bactericides. Alexidine was chosen for further study, as it showed a stronger stabilization activity for PINK1 (C125G) than did chlorhexidine. Alexidine, but not CCCP, induced the accumulation of PINK1 (C125G) on mitochondria (Figure 1, G and H). These results suggest that the identified bactericides somehow prevented OMA1-mediated PINK1 (C125G) degradation.
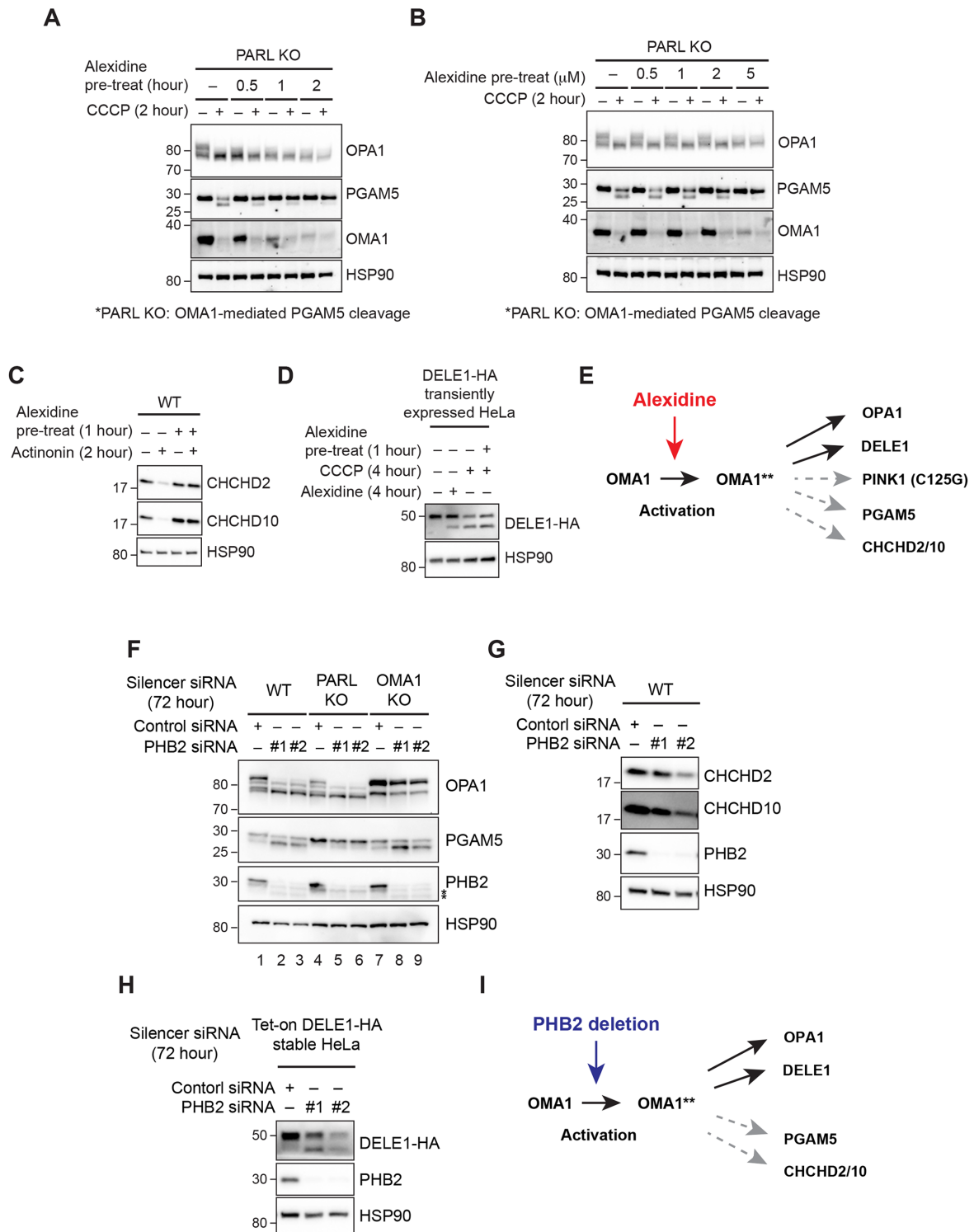
Alexidine demonstrates a substrate-dependent inhibition of OMA1-mediated proteolysis

OMA1 is a stress-responsive protease whose proteolytic activity is enhanced in response to mitochondrial damage including CCCP-induced mitochondrial depolarization (Ehses et al., 2009; Head et al., 2009). OMA1 activation is achieved by its self-cleavage that eventually leads to the complete degradation of OMA1 (Baker et al., 2014; Zhang et al., 2014) (Supplemental Figure S1B). Thus, the degradation of OMA1 indicates its activation. Although chlorhexidine and alexidine appeared to inhibit the OMA1-mediated degradation of PINK1 (C125G) (Figure 1, E and F, PINK1 pan-
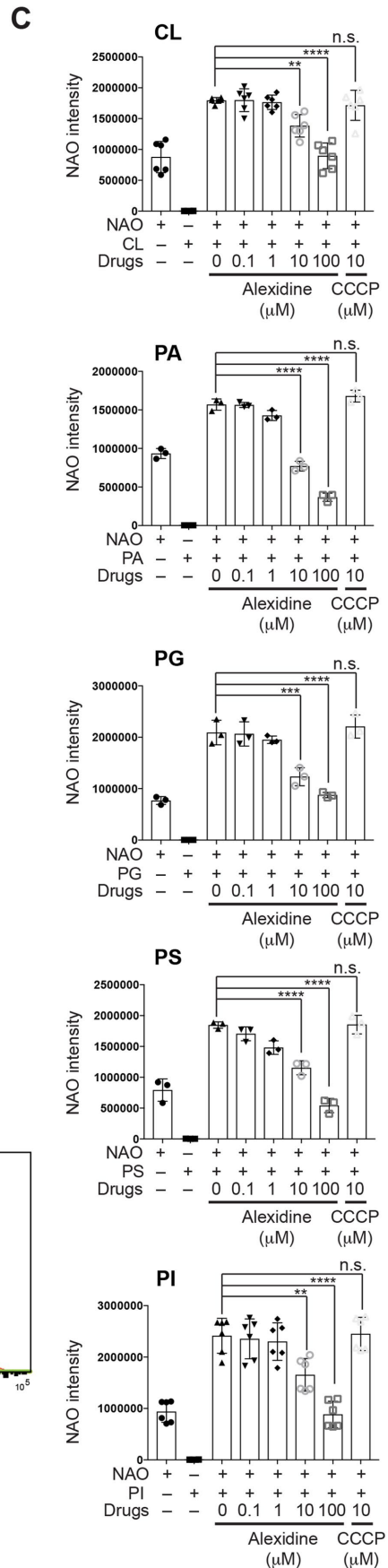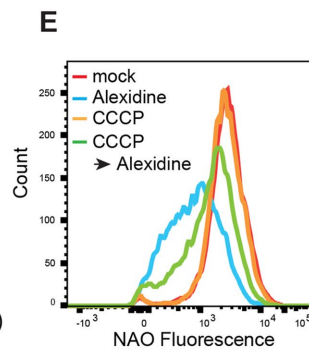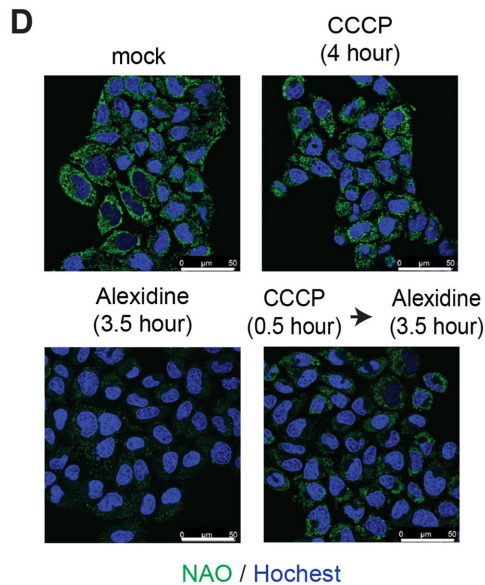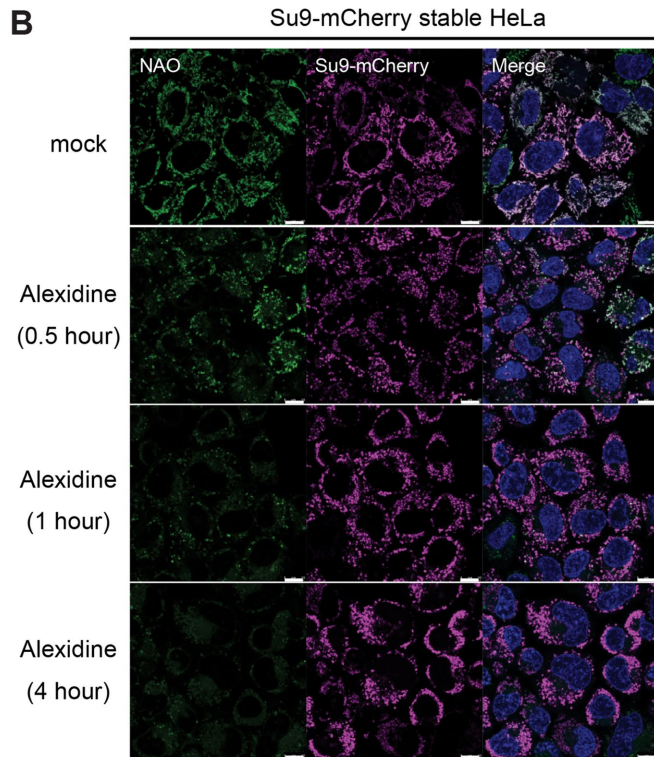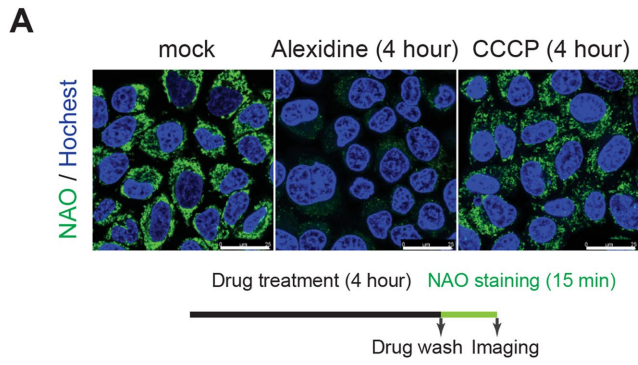
els), we noticed that the autocatalytic degradation of OMA1 was enhanced in response to these bactericides as observed under CCCP-treated conditions (Figure 1, E and F, OMA1 panels). Our previous report suggested that the OMA1 inhibition not only prevented the degradation of PINK1 (C125G) but also restored its kinase activity and thus the subsequent mitochondrial recruitment of Parkin (Sekine et al., 2019). We examined the kinase activity of PINK1 using a previously established method based on a Phos-tag technology (Okatsu et al., 2012). However, treatment with alexidine did not restore the kinase activity of PINK1 (C125G) (Supplemental Figure S1E, lane 7 in the Phos-tag gel).

These results raised the possibility that the bactericide-mediated stabilization of PINK1 (C125G) cannot simply be attributed to the inhibition of OMA1 proteolytic activity. Therefore, we examined the cleavage of other known OMA1 substrates following alexidine treatment. We tested the dynaminlike GTPase OPA1 (Ehses et al., 2009; Head et al., 2009) and the mitochondrial protein phosphatase PGAM5 (Sekine et al., 2012; Wai et al., 2016). It is known that both of these mitochondrial proteins are cleaved in response to CCCP. While CCCP-induced OPA1 cleavage mostly depends on OMA1 (Ehses et al., 2009; Head et al., 2009), CCCP-induced PGAM5 cleavage depends on both OMA1 and PARL (Sekine et al., 2012; Wai et al., 2016). To examine the effect of alexidine on the OMA1-mediated PGAM5 cleavage, we tested whether alexidine pretreatment could inhibit CCCP-dependent PGAM5 cleavage in PARL KO cells. We observed that in PARL KO cells, alexidine pretreatment inhibited CCCP-induced PGAM5 cleavage in a time- and dose-dependent manner (Figure 2, A and B, PGAM5 panels). In contrast, CCCP-dependent OPA1 cleavage was observed even with alexidine pretreatment (Figure 2, A and B, OPA1 panels). These results suggest that alexidine prevented OMA1-mediated PGAM5 cleavage, but not OMA1-mediated OPA1 cleavage. We note that alexidine alone induced the cleavage of OPA1, which is consistent with activation of OMA1 by alexidine. Recently, three other OMA1 substrates were reported: CHCHD2, CHCHD10, and DELE1. CHCHD2 and CHCHD10 are degraded by OMA1 after treatment with actinonin, a mitochondrial translation inhibitor (Liu et al., 2020). DELE1 is cleaved by OMA1 in response to mitochondrial damage including CCCP, which induces the ISR through activation of HRI, one of the eIF2α kinases (Fessler et al., 2020; Guo et al., 2020). Again, alexidine showed a distinct effect on OMA1-mediated proteolysis depending on the particular substrate. Alexidine pretreatment inhibited OMA1-mediated degradation of CHCHD2 and CHCHD10 (Figure 2C), while it failed to inhibit OMA1-mediated cleavage of DELE1 (Figure 2D). Collectively, these results suggest that alexidine is not a simple OMA1 inhibitor (rather, it activates OMA1 itself), but it modulates the OMA1-mediated proteolysis in a substrate-dependent manner (Figure 2E).

To get insights into the substrate dependency, we focused on the IMM prohibitin (PHB) complex. The PHB complex is a heteromeric complex which consists of the closely related IMM-localized proteins, PHB1 and PHB2, and is predicted to form a ringlike structure in the IMM (Tatsuta et al., 2005). It has been shown that the PHB complex may regulate the CL/PE-enriched microdomains in the IMM (Osman et al., 2009a, b; Richter-Dennerlein et al., 2014). Additionally, the PHB complex is known to regulate several IMM-resident proteases including m-AAA (Steglich et al., 1999), OMA1 (Merkwirth et al., 2012; Korwitz et al., 2016), and PARL (Yan et al., 2020). Especially, PHB2 deletion results in the OMA1-mediated cleavage of OPA1 without obvious mitochondrial depolarization (Merkwirth et al., 2008, 2012; Korwitz et al., 2016). As found in these reports, OPA1 cleavage was induced on PHB2 knockdown (KD) in WT cells (Figure 2F, OPA1 panel, lanes 1–3), and it was prevented by OMA1

FIGURE 2: Alexidine shows the substrate-dependent inhibition on OMA1-mediated proteolysis. (A, B) PARL KO HeLa cells were pretreated with alexidine for the indicated time period (A), or at the indicated concentration for 30 min (B), and after, treated with 20 μM CCCP for 2 h. Note that in PARL KO cells, the CCCP-dependent PGAM5 cleavage is mediated by OMA1. The lysate was analyzed by SDS–PAGE. (C) WT HeLa cells were pretreated with 5 μM alexidine for 1 h, and after, treated with 150 μM actinonin for 2 h. The lysate was analyzed by SDS–PAGE. (D) HeLa cells transiently expressed with DELE1-HA was pretreated with 5 μM alexidine for 1 h, and after, treated with 20 μM CCCP for 4 h. The lysate was analyzed by SDS–PAGE. (E) Alexidine showed the inhibitory effect on the OMA1-mediated proteolysis in a substrate-dependent manner. (F–H) The indicated HeLa cells were transfected with control or PHB2 siRNA. After 72 h, cells were harvested, and the lysate was analyzed by SDS–PAGE; 10 μM doxycycline was added for last 24 h to induce DELE1-HA in H. *Nonspecific bands. (I) PHB complex differentially regulates the OMA1-mediated proteolysis in a substrate-dependent manner.

A

mock   Alexidine (4 hour)   CCCP (4 hour)

NAO / Hochest

Drug treatment (4 hour)   NAO staining (15 min)

Drug wash   Imaging

B

Su9-mCherry stable HeLa

NAO   Su9-mCherry   Merge

mock

Alexidine (0.5 hour)

Alexidine (1 hour)

Alexidine (4 hour)

C

CL

PA

PG

PS

PI

D

mock   CCCP (4 hour)

Alexidine (3.5 hour)   CCCP (0.5 hour) ➤ Alexidine (3.5 hour)

NAO / Hochest

E

mock
Alexidine
CCCP
CCCP ➤ Alexidine

deletion (Figure 2F, OPA1 panel, lanes 7–9). PGAM5 cleavage was also induced by PHB2 KD in WT cells (Figure 2F, PGAM5 panel, lanes 1–3). However, unlike OPA1, this was not prevented by OMA1 deletion (Figure 2F, PGAM5 panel, lanes 7–9). Rather, consistent with a recent report (Yan et al., 2020), PARL deletion prevented the PHB2 KD-induced PGAM5 cleavage (Figure 2F, PGAM5 panel, lanes 4–6). We found PHB2 deletion also showed different effects on other OMA1 substrates. PHB2 KD had only slight or no obvious effects on the degradation of CHCHD2 and CHCHD10 (Figure 2G), while it clearly induced DELE1 cleavage (Figure 2H). These results suggest that PHB2 deletion induces the OMA1-mediated proteolysis in a substrate-dependent manner (Figure 2I), which was apparently similar to the effects of alexidine (Figure 2E).

Alexidine has an affinity for the IMM
We next tried to identify a target of alexidine to further address the underlying molecular mechanism of the observed substrate-specific action of alexidine on OMA1-mediated proteolysis. In addition to antimicrobial properties, chlorhexidine and alexidine are also reported as inhibitors of PTPMT1 (Doughty-Shenton et al., 2010), a mitochondrial matrix-localized phosphatase that dephosphorylates phosphatidylglycerol-phosphate, an essential intermediate in CL biosynthesis (Xiao et al., 2011; Zhang et al., 2011). However, KD of PTPMT1 in our PINK1 (C125G)-EYFP stable HeLa cells did not promote PINK1 (C125G) stabilization (Supplemental Figure S2A, lane 5), suggesting that alexidine appears to have a different target in this context.

The proposed mechanism of action of chlorhexidine as a bactericide centers on its bacterial membrane damage-inducing ability through its interaction with phospholipids (McDonnell and Russell, 1999; Cieplik et al., 2019). Alexidine also has a similar activity on the bacterial membranes (McDonnell and Russell, 1999). Guanidinium groups of these compounds possess delocalized positive charges at physiological pH (Langmaier et al., 2016) (Figure 1, C and D). The delocalized positive charges have higher lipophilicity compared with groups that have localized charges, which is considered to confer the efficient binding ability of chlorhexidine and alexidine to phospholipids, together with their long alkyl chain between two symmetric guanidinium groups (McDonnell and Russell, 1999; Cieplik et al., 2019). These observations led us to examine the effect of alexidine on the phospholipids in the IMM. We first tested a phospholipid dye 10-N-Nonyl acridine orange (NAO) staining with or without alexidine treatment. NAO is a lipophilic and positively charged molecule that is often utilized to monitor anionic phospholipids in bacterial membranes (Lin and Weibel, 2016). In eukaryotic cells, NAO selectively accumulates in the IMM (Wolf et al., 2019; Kondadi et al., 2020). Although NAO is originally developed as a CL dye, PTPMT1 deficiency did not alter the mitochondrial NAO staining in HeLa cells (Supplemental Figure S2B), suggesting that NAO has a broader affinity for mitochondrial phospholipid species. We

found that treatment with alexidine but not CCCP dramatically reduced mitochondrial NAO staining (Figure 3A). NAO staining was rapidly lost after alexidine treatment (Figure 3B). In contrast, the fluorescent intensity of Su9-mCherry (matrix marker) was not affected, indicating that mitochondria themselves were still present (Figure 3B). These results indicate that alexidine has effects on the IMM phospholipids. To directly evaluate the binding affinity of alexidine to phospholipids, we examined the effect of alexidine on in vitro binding between NAO and anionic phospholipid species coated on microplate wells (Nomura et al., 2000; Rodriguez et al., 2008). Preincubation with alexidine was found to reduce the fluorescent intensity derived from NAO bound to anionic phospholipids in a dose-dependent manner (Figure 3C). Consistent with the NAO staining in cells (Figure 3A), CCCP did not reduce the NAO intensity in this assay (Figure 3C). A lipidomic analysis of mitochondria isolated from mock- or alexidine-treated cells did not show any decrease in mitochondrial phospholipid species (Supplemental Figure S3), excluding the possibility that alexidine decreased the amount of mitochondria membrane lipids. Altogether, these results suggest that alexidine has an affinity to anionic phospholipids and competes with NAO to bind to these IMM phospholipids.

Intriguingly, the aforementioned chemical property of guanidium groups is also often utilized to target drugs to mitochondria, because it is known to preferentially accumulate in the IMM which has an electrochemical gradient (Sibrian-Vazquez et al., 2008; Battogtokh et al., 2018). Therefore, we tested whether mitochondrial depolarization prevents the action of alexidine on the IMM. CCCP pretreatment partially attenuated the alexidine-induced reduction of NAO staining (Figure 3, D and E). These results suggest that the mitochondrial membrane potential can be a primary driving force for the mitochondrial targeting of alexidine, and the high lipophilicity of alexidine promotes the accumulation of this compound in the hydrophobic lipid environment of the IMM.

Alexidine induces an acute perturbation of IMM integrity
Since alexidine appeared to interact with the IMM phospholipids, we investigated the effects of alexidine on IMM structure and on IMM-shaping proteins. The IMM is structurally subdivided into two domains: the inner boundary membrane (IBM), where the IMM is in close proximity with the OMM, and the cristae, baglike structures where the IMM invaginates into the matrix (Cogliati et al., 2016; Rampelt et al., 2017). These two IMM domains are connected by narrow, necklike structures called cristae junctions (CJs) (Cogliati et al., 2016; Rampelt et al., 2017) (Figure 4A). To examine IMM structure, we performed an electron microscopic (EM) analysis of mitochondria with or without alexidine treatment. The EM images clearly revealed that the IMM structure was severely disrupted after alexidine treatment (Figure 4A, right panels). The alteration of the cristae membrane was the most striking feature. The cristae membrane was

FIGURE 3: Alexidine has an affinity for the IMM. (A and B) WT HeLa cells or HeLa cells stably expressed Su9-mCherry (a matrix marker) were treated with 5 µM alexidine or 20 µM CCCP for the indicated time period. After the drug-treatment, cells were washed with PBS for twice and stained with NAO. NAO staining was analyzed by live-cell imaging. Scale bars; 25 µm (A) and 10 µm (B). (C) NAO fluorescence intensity (Ex 485 nm /Em 535 nm) in individual wells of a microtiter plate which were coated with or without the indicated phospholipid species was measured by microtiter plate reader. Alexidine or CCCP was added at the indicated concentration for 30 min before the NAO staining. Data are shown as mean ± SD ($n = 3$ or $n = 6$ per condition). **$P < 0.01$, ***$P < 0.001$, and ****$P < 0.0001$ (one-way ANOVA followed by Turkey's multiple comparison). (D) WT HeLa cells were treated with 5 µM alexidine, 20 µM CCCP, or the combination of these drugs for the indicated time period. After the drug-treatment, cells were washed with PBS twice and stained with NAO. NAO staining was analyzed by live-cell imaging. Scale bars; 50 µm. (E) FACS analysis of NAO fluorescence intensity in D.
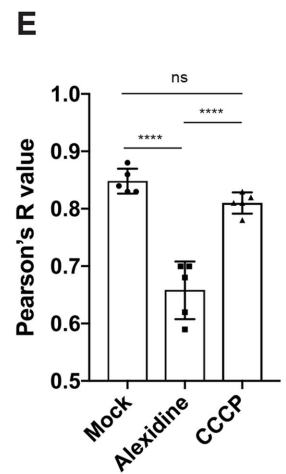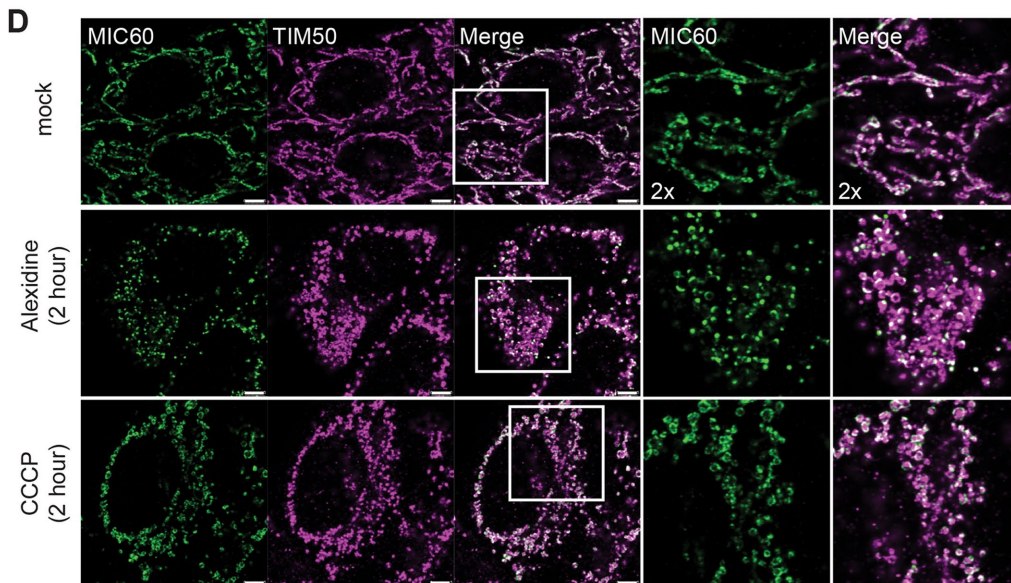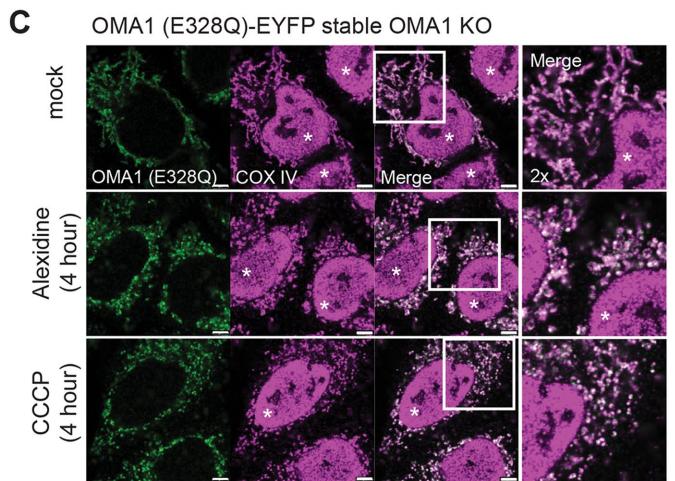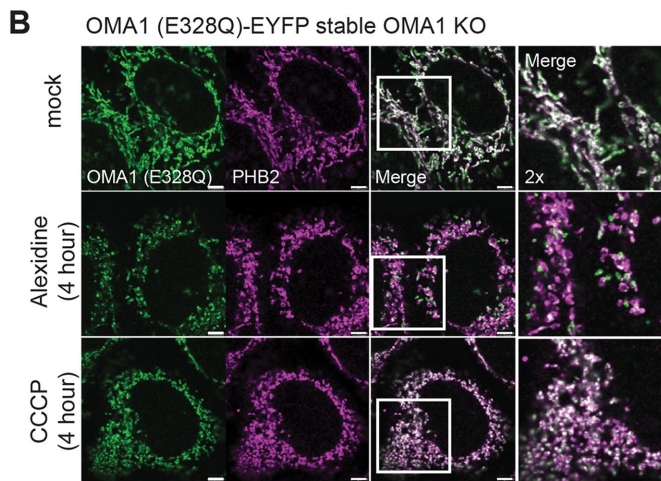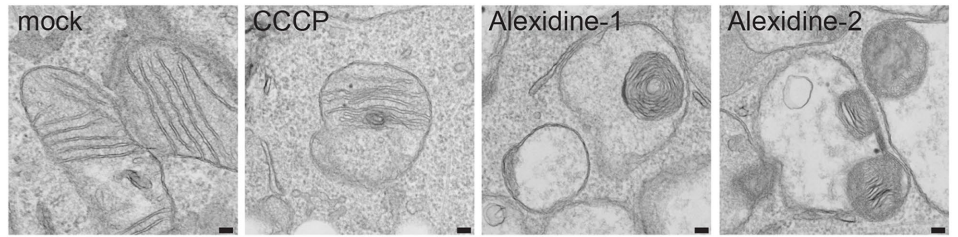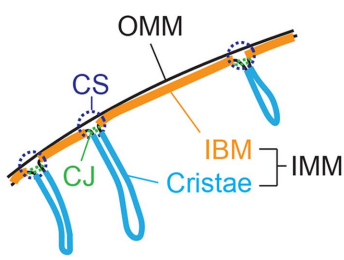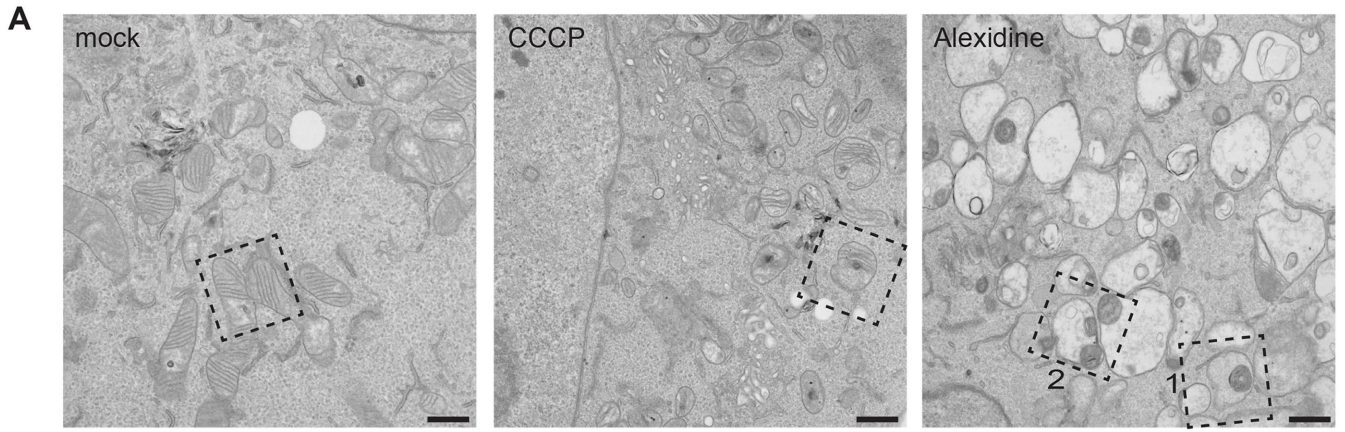
pinched off from the IBM and often appeared bunched up in an onionlike ball in the matrix (Figure 4A, right panels, and Supplemental Figure S4). Mitochondria were swollen and the matrix content seemed to be diluted. However, the OMM and the IBM did not exhibit apparent morphological changes and remained in place, suggesting that alexidine may particularly influence the cristae membranes and CJs. In contrast, CCCP treatment only displayed a mild disturbance in the IMM structure (Figure 4A, middle panels, and Supplemental Figure S4).

We next examined the effects of alexidine on proteins that help shape the IMM. Because we observed substrate-specific effects of alexidine on OMA1-mediated proteolysis (Figure 2E), and PHB2 deletion showed similar effects (Figure 2I), we examined the localization of OMA1 and PHB2. To prevent the stress-dependent autocatalytic degradation of OMA1, we stably expressed an OMA1 protease activity-dead mutant, OMA1 (E328Q) (Sekine *et al.*, 2019), in OMA1 KO cells. The localization of OMA1 and PHB2 mostly overlapped under steady-state and CCCP-treated conditions (Figure 4B, upper and lower panels). However, under alexidine-treated conditions, the localization of these proteins diverged, with part of the OMA1 pool now segregated from the PHB2-positive IMM (Figure 4B, middle panels). When the IMM was stained with Cox IV, a subunit of the cytochrome c oxidase complex, the localization of OMA1 overlapped with the Cox IV-positive IMM even under alexidine-treated conditions (Figure 4C, middle panels), indicating that OMA1 still exists in the IMM.

The MICOS complex is located at CJs where it stabilizes membrane curvature and forms contact sites (CSs) between the OMM and the IMM (Rampelt *et al.*, 2017) (Figure 4A). It is reported that the MICOS complex genetically interacts with the CL synthesis pathway (Hoppins *et al.*, 2011; Friedman *et al.*, 2015), and that some components (Mic60 and Mic27) of the MICOS complex directly bind to CL in vitro (Weber *et al.*, 2013; Michaud *et al.*, 2016). Among the seven components of the metazoan MICOS complex (Rampelt *et al.*, 2017), we examined MIC60 localization before and after the alexidine treatment. Under the resolution of conventional confocal microscopy, MIC60 shows a uniform distribution along the mitochondrial string at steady-state conditions (Figure 4D, upper panels, and Supplemental Figure S5A). However, after alexidine treatment, MIC60 was localized in a restricted region of each fragmented mitochondrion and showed an intense, punctalike localization within the IMM (Figure 4, D and E, and Supplemental Figure S5, A–C). In contrast to the alexidine-treated cells, MIC60 was uniformly distributed in each fragmented mitochondrion after CCCP treatment (Figure 4, D and E, and Supplemental Figure S5, A–C), indicating that the intense MIC60 puncta formation is specifically induced by alexidine. Despite the distribution changes of PHB2 and MIC60, their high weight molecular complex formation was not affected by alexidine treatment (Supplemental Figure S5, D and E). Taken together, these observations suggest that alexidine induced acute redistributions of IMM-resident proteins along with the perturbation of IMM subdomain integrity.

## Alexidine evokes a unique transcriptional/proteostasis signature

From the observations above, we hypothesized that alexidine could be used as an acute mitochondrial membrane damage inducer. Therefore, we decided to characterize the cellular response elicited by the alexidine-induced mitochondrial membrane perturbation. For this purpose, we performed TMT-based quantitative proteomics (Figure 5A, and Supplemental Table S2) and RNA-sequencing analysis (Figure 5C, and Supplemental Table S3). As described so far, alexidine induced mitochondrial alterations that were distinct from CCCP treatment. To identify the proteins or mRNAs whose expression was specifically changed in response to the alexidine-induced mitochondrial membrane stress, we compared three different conditions: mock, alexidine, and CCCP treatment. Gene Ontology analysis for proteins that were significantly changed in the alexidine-treated cells showed a significant enrichment of mitochondria-related proteins (Figure 5B), suggesting that alexidine preferentially affects mitochondria among several other organelles. Many proteins or mRNAs were commonly up-regulated or down-regulated in both the alexidine- and CCCP-treated cells (for example, ISR-targeted genes were up-regulated in both alexidine- and CCCP-treated cells in RNA-seq) (Figure 5, A and C), which may be attributed to the observation that alexidine also induces mitochondrial depolarization at almost the same level as CCCP (Supplemental Figure S1D). Notably, the expression of some proteins was specifically altered in the alexidine-treated cells. Twenty-seven proteins were specifically identified as down-regulated proteins in alexidine-treated cells (fold change < 0.8, *t* test *q* value < 0.05), (Figure 5D and Supplemental Table S2). Among these, 13 proteins were mitochondrial proteins (Figure 5E). These include OXPHOS proteins, proteins which are involved in Coenzyme Q biosynthesis, and PTPMT1. As up-regulated proteins (fold change > 1.5, *t* test *q* value < 0.05), only four nonmitochondrial proteins were specifically up-regulated in response to alexidine (Figure 5F and Supplemental Table S2). These include metallothioneins (MTs) and heme oxygenase 1 (HMOX1), an essential enzyme in heme catabolism (Igarashi and Sun, 2006) (Figure 5G). We next sought to confirm the alexidine-specific expression changes obtained from the proteomics analysis. IB analysis confirmed that HMOX1 was up-regulated while COA7, COX17, and PTPMT1 were down-regulated on alexidine treatment (Figure 5H). Strikingly, these changes were only observed by alexidine treatment and not by other well-known mitochondrial stressors such as CCCP, rotenone (a Complex I inhibitor), actinonin, or CDDO (Figure 5H). We confirmed that each mitochondrial stressor was working in our system by monitoring the OPA1 cleavage and the OMA1 activation on IB (Figure 5H) and mitochondrial ROS production by FACS (Supplemental Figure S6A). CDDO induced the up-regulation of mtHSP60 transcription, one of the targets of mtUPR (Munch and Harper, 2016), but alexidine did not show any enhancement of mtHSP60 transcription (Supplemental Figure S6B). RNA-seq results and real-time (RT)-PCR analysis revealed that the up-regulation of HMOX1 and MT2A was induced at the transcriptional level (Figure 5G and

---

FIGURE 4: Alexidine induces an acute perturbation of IMM integrity. (A) The EM images of the WT HeLa cells that were treated with DMSO, 20 μM CCCP, or 5 μM alexidine for 4 h. Scale bars; 800 nm (upper panels), 100 nm (lower panels). (B, C) OMA1 KO cells stably expressed OMA1 (E328Q)-EYFP were treated with 5 μM alexidine or 20 μM CCCP for 4 h and subjected to ICC. Cox IV was used as a typical IMM marker protein (C). *Nonspecific signal. Scale bars; 5 μm. (D) WT HeLa cells were treated with 5 μM alexidine or 20 μM CCCP for 2 h and subjected to ICC. TIM50 was used as a typical IMM marker protein. Scale bars; 5 μm. (E) Pearson's R values between MIC60 and TIM50 fluorescent signals from five images for each condition in D were analyzed using Image J. Data are shown as mean ± SD (*n* = 5 per condition). ****P < 0.0001 (one-way ANOVA followed by Turkey's multiple comparison).

A TMT-proteomics (Alexidine vs. CCCP)
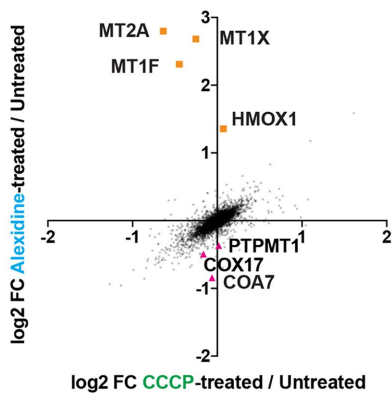
B Fischer Exact test (Mock vs. Alexidine)
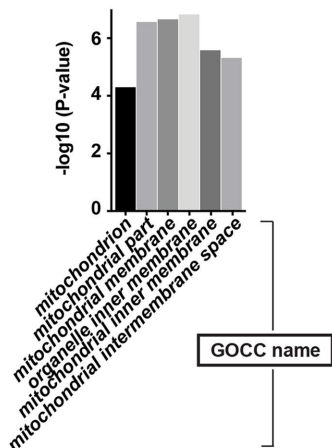
C RNA-seq (Alexidine vs. CCCP)
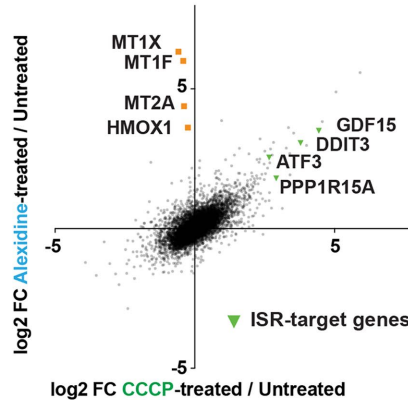
D **Down**-regulated proteins
(fold change < 0.8, T-TEST q-value < 0.05)
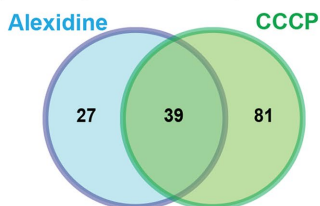
F **Up**-regulated proteins
(fold change > 1.5, T-TEST q-value < 0.05)
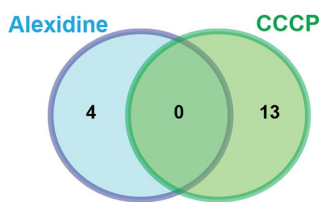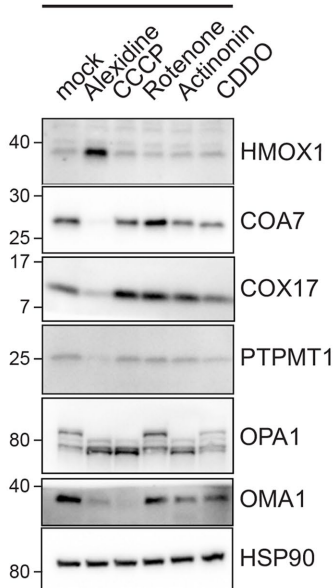
E

Biological pathways		Gene names	Fold change of protein (Alexidine / Untreated)	Fold change of mRNA (Alexidine / Untreated)	Localization
OXPHOS	Complex I	NDUFAF4	0.78	0.94	matrix
		NDUFA8	0.75	0.84	IMS
	Cytochrome C	CYCS	0.62	0.88	IMS
	Complex IV	COA4	0.74	0.78	IMS
		COA6	0.78	0.85	IMS
		COA7	0.55	0.95	IMS
		COX17	0.71	0.86	IMS
Coenzyme Q biosynthesis		COQ5	0.78	1.17	matrix
		COQ7	0.76	1.13	matrix
Cardiolipin synthesis		PTPMT1	0.77	0.91	matrix
Others		GLRX2	0.63	1.06	matrix
		ENDOG	0.68	0.93	IMS
		PYURF	0.75	0.88	?

Fold change of protein or mRNA :
0.5 — 1.0
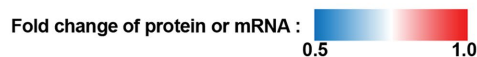
G

Biological pathways	Gene names	Fold change of protein (Alexidine / Untreated)	Fold change of mRNA (Alexidine / Untreated)
Heavy metal detoxification	MT2A;MT1G	6.96	20.7
	MT1X	6.42	80.4
	MT1F	4.95	63.9
Heme catabolism	HMOX1	2.56	12.2

H Drug treatment (8 hour)

I
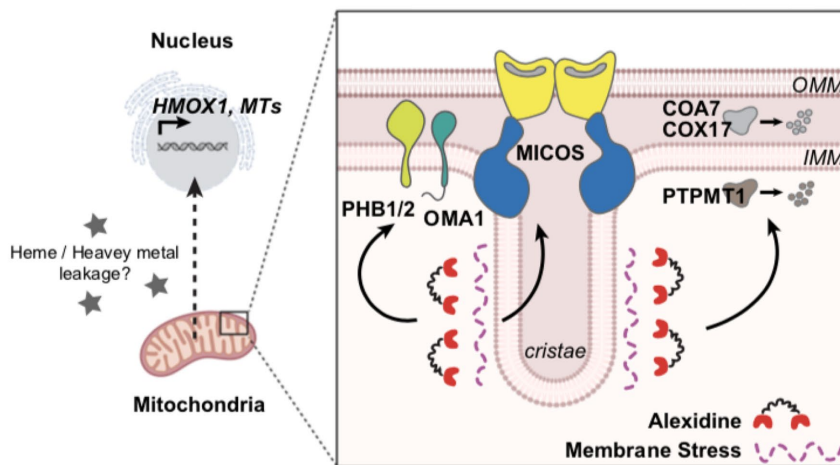
Supplemental Figure S6C), indicating the existence of a mitochondrial-nuclear communication in response to alexidine treatment. In contrast, the mRNA levels of the alexidine-specific down-regulated mitochondrial proteins including COA7 and COX17 did not significantly change after alexidine treatment, indicating that alexidine likely induces the posttranscriptional degradation of these proteins (Figure 5E and Supplemental Figure S6C). LONP KD prevented the alexidine-induced down-regulation of PTPMT1 (Supplemental Figure S6D), suggesting that at least PTPMT1 is degraded within the mitochondria. Consistent with the observation that PTPMT1 deficiency affected neither PINK1 (C125G) accumulation nor the NAO staining unlike alexidine (Supplemental Figure S2), it did not show the induction of HMOX1 or the degradation of COA7 (Supplemental Figure S6E).

Collectively, our results suggest that alexidine can evoke unique mitochondrial responses that are not induced by other typical mitochondrial stressors, presumably through the perturbation of the IMM integrity (Figure 5I).

DISCUSSION
In this study, we found two bactericides, chlorhexidine and alexidine, as small molecules that can induce the acute perturbation of mitochondrial membrane integrity. EM analysis of mitochondria after alexidine treatment showed a strikingly altered cristae membrane structure, while keeping the OMM and the IBM largely in place (Figure 4A). This suggests that alexidine can specifically damage the cristae among several distinct membrane compartments within mitochondria (Figure 5I). It has been noted that cristae membranes are the membranes where OXPHOS proteins are concentrated (Cogliati *et al.*, 2016). Our TMT-based quantitative proteomics analysis indicated that many OXPHOS proteins were down-regulated after alexidine treatment (Figure 5E), which also supports the specific action of alexidine on the cristae membrane. Interestingly, several recent studies identified alexidine (and chlorhexidine) as an agent that can alter cellular metabolism. This metabolic shift ultimately resulted in various effects on cells: the anti-invasive and metastatic activity on tumor cells (Kenny *et al.*, 2015; Commander *et al.*, 2020), the maintenance of the quiescent status of stem cells (Liu *et al.*, 2015), the enhanced glucose utilization in vivo (Nath *et al.*, 2015), or the transcription factor TFEB nuclear translocation through AMPK activation (Wang *et al.*, 2017). Some of these reports found that the alexidine treatment reduced oxygen consumption (Liu *et al.*, 2015) and preferentially shifted the energy source from OXPHOS to glycolysis (Commander *et al.*, 2020). Because PTPMT1 was reported as a metazoan target of alexidine (Doughty-Shenton *et al.*, 2010), some studies indicated above speculated that the observed metabolic effects may result from PTPMT1 inactivation. However, the cristae membrane-disrupting activity of alexidine, which we identified in this study, must now be considered as a basis for the acute effects of alexidine on the cellular metabolism.

It still remains elusive how alexidine specifically affects the cristae membrane. As predicted from the chemical properties of guanidium groups of alexidine (Sibrian-Vazquez *et al.*, 2008; Battogtokh *et al.*, 2018), our NAO staining assay indicated that mitochondrial membrane potential can be a driving force for the mitochondrial targeting of alexidine (Figure 3, D and E). Because of the high abundance of OXPHOS proteins in the cristae (Cogliati *et al.*, 2016), the cristae membranes have higher membrane potential than the IBM (Wolf *et al.*, 2019). This unique feature of the cristae may explain the specific effect of alexidine on this membrane compartment within the IMM. Also, it has been suggested that the high curvature of the cristae is created by high amounts of nonbilayer lipids such as CL and PE (Horvath and Daum, 2013; Cogliati *et al.*, 2016). We demonstrated that alexidine has a reasonable affinity for CL as it is able to compete with NAO (Figure 3C). Therefore, this property of alexidine may also contribute to the accumulation of alexidine in the cristae membrane.

As a result of alexidine treatment, we observed a robust induction of HMOX1, a heme-degrading enzyme, and several MTs, metal chelators (Figure 5, F–H). The direct link between the alexidine-mediated mitochondrial membrane damage and the induction of HMOX1 and MTs is not known. Early studies indicate that HMOX1 and MTs are simultaneously induced by heme addition to the culture media (Smith, 2000). Subsequent studies have demonstrated that HMOX1 induction was mediated by nuclear factor erythroid 2-related factor 2, a transcription factor involved in the antioxidant response (Igarashi and Sun, 2006). Mitochondria are known as a site for heme biosynthesis (Xu *et al.*, 2013). Also, the mitochondrial matrix has a pool of heavy metal copper (Xu *et al.*, 2013). Together with Fe-S clusters that are synthesized in mitochondria, heme and copper are utilized as important cofactors for various enzymes including OXPHOS proteins. Due to their harmful radical-formation activity, the export of newly synthesized heme across the mitochondrial membranes is tightly regulated by a membrane-embedded heme exporter, while copper chaperones ensure the safe delivery of

---

FIGURE 5: Alexidine evokes a unique transcriptional/proteostasis signature. (A, B) WT HeLa cells were treated with 5 µM alexidine or 20 µM CCCP for 8 h and subjected to TMT-based quantitative proteomics. Scatter plot for Log$_2$ FC of protein amount in CCCP treated/untreated (*x*-axis) and Log$_2$ FC of protein amount in alexidine treated/untreated (*y*-axis) (A). Values are from Supplemental Table SS2. The enrichment analysis of proteins whose amount was significantly changed (t test *q* value < 0.05) in the alexidine-treated cells compared with the mock-treated cells (B). The enriched Gene Ontology Cellular Component (GOCC) classes and each enrichment value was shown. (C) WT HeLa cells were treated with 5 µM alexidine or 20 µM CCCP for 4 h and subjected to RNA-seq analysis. Scatter plot for Log$_2$ FC of mRNA amount in CCCP treated/untreated (*x*-axis) and Log$_2$ FC of mRNA amount in alexidine treated/untreated (*y*-axis). Values are from Supplemental Table SS3. (D) Venn diagram of down-regulated proteins (fold change < 0.8, t test *q* value < 0.05) after the alexidine or CCCP treatment in A. (E) List of the alexidine-specific down-regulated mitochondrial proteins in A. Fold change of mRNA level of each protein was obtained from RNA-seq results in C. IMS; inner membrane space. (F) Venn diagram of up-regulated proteins (fold change > 1.5, t test *q* value < 0.05) after the alexidine or CCCP treatment in A. (G) List of the alexidine-specific up-regulated proteins in A. Fold change of mRNA level of each protein was obtained from RNA-seq results in C. (H) Validation of TMT-based proteomics results by SDS–PAGE. WT HeLa cells were treated with the indicated drugs for 8 h (5 µM alexidine, 20 µM CCCP, 10 µM rotenone, 150 µM actinonin, and 10 µM CDDO) and subjected to further analyses. (I) Graphical summary of this study. See text for detail.

copper to target proteins (Xu *et al.*, 2013). It is possible that the alexidine-mediated IMM perturbation disturbed this regulation and resulted in the heme and copper leakage from mitochondria. Ultimately, it might lead to the induction of HMOX1 and MTs as a preventive strategy. Complex IV utilizes a heme-copper center to reduce oxygen (Xu *et al.*, 2013). We observed that the alexidine treatment strongly degraded two Complex IV assembly factors, COA7 and COX17 (Xu *et al.*, 2013; Kozjak-Pavlovic *et al.*, 2014; Mohanraj *et al.*, 2019) (Figure 5H). The exact role of COA7 in the assembly of Complex IV was not known, but very recently, its heme-binding/chaperoning activity was proposed (Formosa *et al.*, 2021). COX17 is well known as a copper chaperone that delivers copper to Complex IV (Xu *et al.*, 2013). Therefore, in addition to the direct leakage of heme and copper from the mitochondria, it is also possible that heme and copper released from degraded OXPHOS proteins activate the transcription of HMOX1 and MTs. In either case, the induction of HMOX1 and MTs can be used as a sensitive marker of the mitochondrial membrane damage.

In addition to these transcriptional/proteostasis alterations, alexidine remodeled the IMM-resident membrane proteins including PHB2, OMA1, and MIC60 (Figure 4, B and D). The single particle EM analysis of PHB complex suggested that it forms a ringlike structure in the IMM (Tatsuta *et al.*, 2005). It is predicted that the ringlike PHB complex can exert a partitionlike function in the IMM, where it can define the lateral distribution of specific lipids, including CL and PE, or proteins such as IMM-resident proteases including OMA1 (Osman *et al.*, 2009b). As alexidine showed an affinity to CL (Figure 3C), alexidine might be able to accumulate in the PHB complex-organized CL/PE-enriched domain of the IMM. Previous reports revealed that PHB deletion can activate OMA1 proteolytic activity and induce subsequent OPA1 cleavage without mitochondrial membrane depolarization (Merkwirth *et al.*, 2008; Merkwirth *et al.*, 2012; Korwitz *et al.*, 2016), indicating that PHB complex may hold OMA1 in the inactive state presumably through restricting the protease to specific IMM microdomains. We observed the segregation of OMA1 from PHB2-positive IMM after alexidine treatment (Figure 4B). These observations may indicate that alexidine causes OMA1 to dissociate from the PHB complex-organized microdomain and that once OMA1 is released from PHB complex-mediated inhibition, it is proteolytically active. However, OMA1 did not cleave or degrade certain substrates such as PINK1 (C125G), PGAM5, CHCHD2, and CHCHD10 on alexidine treatment (Figure 2E). PHB2 deletion provided similar results (Figure 2I). These observations may imply the existence of an additional layer of regulation that allows OMA1 to access some substrates.

MIC60, one of the important components of the MICOS complex (Rampelt *et al.*, 2017), showed a punctalike localization within the IMM after alexidine treatment (Figure 4, D and E, and Supplemental Figure S5, A–C). Among several components of the MICOS complex, it has been suggested that Mic60 can self-assemble and form puncta within the IMM when all other MICOS components are absent in yeast (Friedman *et al.*, 2015). Moreover, the recent analysis showed the de novo formation of CJs by drug-controlled expression of MIC60 in reconstituted MIC60 KO cells (Stephan *et al.*, 2020), establishing a critical role for MIC60 in CJ formation. Upstream determinants of MIC60 localization are not fully understood. However, recent studies in yeast have revealed that the aforementioned Mic60 puncta formed in the absence of other components of the MICOS complex are often observed in proximity to ER-mitochondria CSs, where the ERMES complex exists (Tirrell *et al.*, 2020). The ERMES complex physically tethers the ER and mitochondria in yeast and creates membrane CSs to allow efficient lipid transfer between the ER and the mitochondria (Tamura *et al.*, 2020). Together with the fact that MICOS and ERMES genetically interact with each other (Hoppins *et al.*, 2011), cooperative functions of MICOS and ERMES have been suggested in mitochondrial membrane architecture (ERMIONE) (van der Laan *et al.*, 2012). Mitochondrial lipid homeostasis depends on both interorganelle (mainly from the ER) and intraorganelle (between the OMM and the IMM) lipid trafficking (Tatsuta and Langer, 2017; Tamura *et al.*, 2020). Therefore, the coordinated regulation of ERMES-MICOS localization may be functionally linked to allow for efficient lipid trafficking across the membranes. Although it has not been examined whether the MICOS complex is involved in interorganelle lipid trafficking, it is known that the MICOS complex is involved in intramitochondrial lipid metabolism (Aaltonen *et al.*, 2016; Michaud *et al.*, 2016). Our EM analysis revealed that the cristae structure was severely damaged following alexidine treatment (Figure 4A and Supplemental Figure S4). In such a case, it is expected that mitochondrial lipid demand is significantly increased in order to help restore the highly folded cristae structure. It is tempting to speculate that the alexidine-induced MIC60 puncta formation plays a role in this process as part of a mitochondrial membrane stress response. However, we cannot deny the possibility that the distribution change of MIC60 is a consequence of the cristae disruption. It may be also of note that several reports indicate a link between the MICOS complex and the COA7 or COX17 (robustly degraded proteins after the alexidine treatment). For example, in yeast, it was shown that Cox17 physically interacts with Mic60 and modulates the MICOS complex formation (Chojnacka *et al.*, 2015). Other studies suggest that the sustained KD of MIC60 (or its interactor, SAM50) resulted in the degradation of COA7 in mammalian cells (Kozjak-Pavlovic *et al.*, 2014). COA7 was also identified as the possible interactor of MIC10, another important component of MICOS complex (Alkhaja *et al.*, 2012). These previous observations may explain the reason why we observed the relatively specific and robust degradation of COA7 and COX17 among over 100 components of OXPHOS system.

In conclusion, we discovered alexidine and chlorhexidine as small molecules that enable us to acutely and preferentially perturb the mitochondrial membrane architecture in the IMM (Figure 5I). Our findings therefore offer a useful chemical-biological tool for delineating mitochondrial membrane stress responses.

MATERIALS AND METHODS

Cell culture, transfection, and treatments

HEK293T and HeLa cells were cultured in DMEM (Life Technologies) supplemented with 10% fetal bovine serum (VWR Life Science), 10 mM HEPES (Life Technologies), 1 mM sodium pyruvate (Life Technologies), nonessential amino acids (Life Technologies), and GlutaMAX (Life Technologies). For RNA interference, 20 nM Stealth siRNAs (Steath RNAi Negative Control Med GC Duplex #2, 12935112; LONP, HSS113887) (Thermo Fisher Scientific) or 5 nM Silencer select siRNAs (Silencer Select Negative Control #1 siRNA, 4390843; OMA1, s41776; LONP, s17903; PTPMT1, s229947) (Thermo Fisher Scientific) were transfected using Lipofectamine RNAi max transfection reagent (Thermo Fisher Scientific) at the same time as cell seeding. For drug treatment experiments, cells were incubated in medium containing one or more of the following compounds: CCCP (Cayman Chemical), MG132 (Sigma), chlorhexidine (Cayman Chemical), alexidine (Cayman Chemical), rotenone (Cayman Chemical), actinonin (Cayman Chemical), CDDO (Cayman Chemical). For examination of mitochondrial membrane potential or mitochondrial ROS production, 20 nM TMRM (Thermo Fisher Scientific) or 50 nM MitoSOX (Thermo Fisher Scientific), respectively, was directly added

to cell culture media and incubated for 15 min. For NAO staining, cells were washed twice with phosphate-buffered saline (PBS) and incubated with 100 nM NAO (Thermo Fisher Scientific) for 15 min. Cells were washed and replaced with normal medium followed by live-scell imaging using a 63×/1.4 NA oil immersion objective on a Leica SP8 LIGHTNING confocal microscope (Leica) or FACS analysis using Attune NxT Acoustic Focusing Cytometer (Thermo Fisher Scientific).

Plasmids

Site-directed mutagenesis of pLenti-CMV-Neo-PINK1 (C125G)-EYFP or pLVX-puro-OMA1 (E328Q)-EYFP was performed by PCR amplification (CloneAmp HiFi PCR Premix, Takara or Q5 High-Fidelity DNA Polymerase system, NEB) of PINK1 or OMA1 encoding plasmid using appropriate primers followed by Gibson assembly (In-Fusion HD Cloning system, Clontech) into the *Sal*I-*Xho*I of the pLenti-CMV-Neo vector, or into the *Eco*RI site of pLVX-puro vector (Clontech). pLVX-puro-DELE1-HA and pLVX-puro-Su9-mCherry was created by PCR amplification and subcloning into the *Eco*RI site of pLVX-puro vector. pRetroX-Tight-puro-DELE1-HA was created by PCR amplification and subcloning into the *Bam*HI/*Not*I site of pRetroX-Tight-puro vector (Clontech). All constructs were confirmed by DNA sequencing.

Generation of stable cell lines

To generate stably transfected cell lines, lentiviruses (for plasmids within pLenti-CMV-neo or pLVX-puro vectors) and retroviruses (for plasmids within pRetroX-Tight-puro vector) were packaged in HEK293T cells. HeLa cells were transduced with viruses with 10 μg/ml polybrene (Sigma) then optimized for protein expression via antibiotics selection. PINK1 KO HeLa cells stably expressed PINK1 (WT)-EYFP or PINK1 (C125G)-EYFP were monocloned, and clone #21 or clone #23, respectively, was used in this study. For generating the Tet-on DELE1-HA stable cell line, Retro-X-Tet-on Inducible Expression System (Clontech) was used according to the manufacturer's instruction.

Generation of KO cell lines

PTPMT1 KO HeLa cell lines were generated using lentiCRISPRv2 system (Sanjana *et al.*, 2014; Shalem *et al.*, 2014). Briefly, after the infection of lentiviruses that express hSpCas9 and PTPMT1 sgRNA (5′-TGGCGCGTCAAGCTCCGCAA-3′), infected cells were selected via the treatment with 500 μg/ml hygromycin (Sigma) for 24 h. The selected cells were cultured for more than 2 wk at least to ensure the efficient gene deletion and used in experiments. The following HeLa KO cell lines were kindly provided by Richard J. Youle (NIH, NINDS): PINK1 KO (Nezich *et al.*, 2015), OMA1 KO (Sekine *et al.*, 2019), and PARL KO (Sekine *et al.*, 2019).

Immunoblotting (IB)

For SDS–PAGE, cells were lysed with 1× NuPAGE LDS sample buffer (Thermo Fisher Scientific) supplemented with 100 mM dithiothreitol (DTT) (Sigma) and boiled with shaking for 15 min. Approximately, 50 μg of protein per sample was separated on 7.5, 10, or 4–20% gradient Mini-PROTEAN TGX Precast Gel (Bio-Rad) or Criterion TGX Gels (Bio-Rad) and then transferred to a nitrocellulose membrane (Bio-Rad) or PVDF membrane (Bio-Rad). The membrane was blocked with Odyssey Blocking Buffer (LI-COR) and incubated with the indicated primary antibodies at 4°C overnight. After washing with PBS-T (PBS + 0.05% Tween-20), the membrane was incubated with HRP–conjugated secondary antibodies (Thermo Fisher Scientific) and washed again with PBS-T. Detection was performed with iBright

CL1000 Imaging System (Thermo Fisher Scientific). For Phos-tag SDS–PAGE, cells were lysed with 1% Triton buffer [1% Triton X-100, 150 mM NaCl, 50 mM Tris-HCl, pH 7.4, 1 mM EDTA, phosphatase inhibitors (PhosSTOP, Sigma), and protease inhibitors (cOmplete, Sigma)]. After centrifugation, the lysate that contains 10 μg of protein per sample was mixed with 2× Laemmli sample buffer (Bio-Rad) supplemented with 2 M 2-mercaptoethanol (Bio-Rad) and boiled for 3 min. Samples were separated on 7.5% Mini-Gel (TGX FastCast Acrylamide Solutions, Bio-Rad) containing 50 μM Phos-tag AAL-107 (Wako) and 10 mM $MnCl_2$ (Sigma) according to the manufacturer's instructions. For the elimination of the manganese ion from the gel, the gel was soaked with a transfer buffer containing 1 mM EDTA for 10 min, washed with a transfer buffer without EDTA for 10 min, and then transferred to a PVDF membrane (Bio-Rad).

Immunocytochemistry (ICC)

Cells were seeded into Lab-Tek Chambered Coverglass with 4 wells (Thermo Fisher Scientific). Cells were rinsed in PBS and fixed with PBS containing 4% formaldehyde for 15 min at room temperature. Cells were permeabilized with PBS containing 0.1% Triton X-100 for 10 min at room temperature. Blocking was performed using PBS containing 2% bovine serum albumin (BSA) for 30–60 min at room temperature. For immunostaining, cells were incubated with primary or secondary antibodies (Alexa Fluor, Thermo Fisher Scientific) diluted in PBS containing 2% BSA overnight at 4°C or about 2 h at room temperature, respectively. Cells were imaged using a 63×/1.4 NA oil immersion objective on Leica SP8 LIGHTNING confocal microscope (Leica).

Antibodies

The following antibodies were used in IB or ICC: PINK1 (Cell Signaling, 6946S), OMA1 (Santa Cruz, sc-515788), PGAM5 (Thermo Fisher Scientific, PA5-57894), CHCHD2 (Proteintech, 66302-1-lg), CHCHD10 (Sigma, HPA003440), OPA1 (BD Biosciences, 612607), HSP90 α/β (Santa Cruz, sc-7947 or sc-13119), HSP60 (Santa Cruz, sc-13115), Tim50 (Santa Cruz, sc-393678), Tom20 (Santa Cruz, sc-17764), PHB2 (Proteintech, 66424-1-lg) for ICC, PHB2 (Proteintech, 12295-1-1g) for IB, Cox IV (Thermo Fisher Scientific, PA5-19471), Mic60 (Proteintech, 10179-1-AP), HMOX1 (GeneTex, GTX101147), PTPMT1 (Santa Cruz, sc-390901), COX17 (Proteintech, 11464-1-AP), COA7 (Proteintech, 25361-1-AP), LONP (Novus Biologicals, NBP1-81734), GFP (Novus Biologicals, NB600-597 or NB-600-308), and HA (Cell Signaling, 3724).

FDA-approved compound library screening

The FDA-approved compound library (Selleck, 100 nl per drug) was stamped to black 384-well plates with glass bottoms using CyBio Well vario (Analytik Jena). PINK1 KO HeLa cells stably expressed PINK1 (C125G)-EYFP (clone #23) were then added to give density of 4000 cells per well and a final drug concentration of 5 μM. After 18 h of treatment, CCCP was added to a final concentration of 20 μM and incubated for 4 h followed by fixation in 4% paraformaldehyde and counterstaining with Hoechst 33342. Fluorescence was detected using an ImageXpress Micro XLS (Molecular devices) high-content imager and the cellular EYFP fluorescence signal was calculated using CellProfiler software (McQuin *et al.*, 2018).

In vitro NAO assay

Binding of NAO to each anionic phospholipid was studied in lipid monolayers (Nomura *et al.*, 2000; Rodriguez *et al.*, 2008), with slight modifications; 96-well microtiter plates (Corning, 3915) were coated with 50 μl of 20 μM each anionic phospholipid

in ethanol and evaporated at 37°C for 5 h. An increasing concentration of alexidine (final; 0–100 µM) or CCCP (final; 10 µM) in 50 µl PBS containing 2% BSA was added and incubated at 37°C for 30 min. Then, NAO (final; 100 nM) in 50 µl PBS containing 2% BSA was added and incubated at 37°C for 30 min protected from light. After the incubation, each well of the plates was washed with 150 µl PBS for five times. Finally, NAO fluorescence intensity was measured by SpectraMax i3x Multi-Mode Detection Platform (Molecular Devices) using Ex 485 nm/Em 535 nm. The following anionic phospholipids purchased from Avanti Polar Lipids were used: Heart CA (840012P), Egg PA (840101P), Egg PG (841138P), Liver PI (840042P), and Brain PS (840032P).

Transmission EM
HeLa cells were fixed with 4% glutaraldehyde (Electron Microscopy Services) in EM buffer (0.1 N sodium cacodylate at pH 7.4 with 2 mM calcium chloride) for 30 min at room temperature and then at 4°C for at least 24 h. Samples were washed with buffer and treated with 1% osmium tetroxide in 0.1 N cacodylate buffer at pH 7.4 for 1 h on ice, washed, and en bloc stained with 0.25–1% uranyl acetate in 0.1 N acetate buffer at pH 5.0 overnight at 4°C, dehydrated with a series of graded ethanol, and finally embedded in epoxy resins. Ultrathin sections (70 nm) were stained with lead citrate and imaged with a JEOL 1200 EXII Transmission electron microscope.

RNA isolation and RT PCR
Total RNAs were isolated using RNeasy Mini Kit (Qiagen) and reverse-transcribed to cDNA using iScript cDNA Synthesis Kit (Bio-Rad) according to the manufacturer's instructions. RT PCR was performed using SYBR Green Master Mix (Bio-Rad) and QuantStudio 3 RT-PCR system (Thermo Fisher Scientific). All expression levels were normalized to that of RPS18 mRNA. The following RT-PCR primers were used: RPS18, (forward) 5'-cttccacaggaggcctacac-3' and (reverse) 5'-cgcaaaatatgctggaacttt-3'; HMXO1, (forward) 5'-ggcagagggt-gatagaagagg-3' and (reverse) 5'-agctcctgcaactcctcaaa-3'; MT2A, (forward) 5'-aacctgtcccgactctagcc-3' and (reverse) 5'-Gcaggtgcag-gagtcacc-3'; COA7, (forward) 5'-gcaggtcaagtccttttttgg-3' and (reverse) 5'-ccaccagccgatagcaac-3'; COX17, (forward) 5'-aagatgccgggtctg-gtt-3' and (reverse) 5'-ttcttctctctttctcgatgataca-3'; mtHSP60, (forward) 5'-cctgcactctgtccctcact-3' and (reverse) 5'-gggtaaccgaagcatttctg-3'.

BN-PAGE
BN-PAGE analysis was performed according to manufacturer's instruction with some modifications. Briefly, the samples were harvested using a Native PAGE Sample Prep Kit (Invitrogen). Cells were extracted with 1× Native PAGE buffer containing 1% digitonin and protease inhibitors (cOmplete, Sigma) for 15 min at 4°C, pipetted up and down 10 times, and centrifuged at 14,000 × g for 30 min at 4°C. Samples were separated on NativePAGE 3–12% Bis-Tris Mini Protein Gel (Invitrogen) using Native PAGE Running Buffer (Invitrogen) containing 0.002% G-250 (Invitrogen). For IB analysis, gels were shaken in denaturation buffer (10 mm Tris-HCl, pH 6.8, 1% SDS, and 0.006% 2-mercaptoethanol) for 15 min at 60°C after electrophoresis and then transferred to PVDF membranes.

RNA-seq
RNA-seq was performed by MedGenome.

Illumina TruSeq stranded mRNA kit was used to prepare libraries according to the manufacturer's instructions. Resulting libraries were sequenced on NovaSeq 6000 using paired-end 100 base pair sequencing at the depth of 40-M reads per sample.

TMT-based quantitative proteomics
TMT-based quantitative proteomics was performed by MS Bioworks.

Sample preparation. Cells were lysed in 8 M urea, 50 mM Tris-HCl (pH 8.0), 1× complete protease inhibitor (Roche), and 1× PhosStop (Roche) with a sonic probe (3 × 30 s at 80% amplitude) with subsequent mixing at room temperature for 1 h at 1000 rpm on a Thermomixer. Lysates were quantified by Qubit fluorometry (Life Technologies); 50 µg of each sample was digested overnight with trypsin. Briefly, samples were reduced for 1 h at room temperature in 12 mM DTT followed by alkylation for 1 h at room temperature in 15 mM iodoacetamide. Trypsin was added to an enzyme:substrate ratio of 1:20. Each sample was acidified in formic acid and subjected to SPE on an Empore SD C18 plate. Each sample was lyophilized and reconstituted in 140 mM HEPES (pH 8.0), 30% acetonitrile for TMT labeling. Peptides were labeled using TMT 10-plex (Thermo Fisher Scientific) according to the manufacturer's instructions. Briefly, 40 µl of acetonitrile was added to each TMT tag tube and mixed aggressively. Tags were incubated at room temperature for 15 min; 30 µl of label was added to each peptide sample and mixed aggressively. Samples were incubated in an Eppendorf Thermomixer at 300 rpm at 25°C for 1.5 h. Reactions were terminated with the addition of 8 µl of fresh 5% hydroxylamine solution and 15 min incubation at room temperature. Each labeled sample was pooled, frozen, and lyophilized and subjected to SPE on a High-Density 3M Empore SDB-XC column. The eluent was lyophilized. Peptides were fractionated using high pH reverse-phase chromatography on an Agilent 1100 HPLC system using a Waters XBridge C18 column (2.1 mm ID × 150 mm length, 3.5-µm particle size) at 300 µl/min. The following gradient was employed: 0.5% B initial conditions, 0.5–3.0% B from 0 to 1 min, 3–25% B from 1 to 36 min, 25–45% B from 36 to 44 min, 45–90% B from 44 to 47 min, 90% B from 47 to 49 min, and 90–0.5% buffer B from 49 to 50 min (buffer A: 100% H_2O, 10 mM NH_4OH; buffer B: 100% CH_3CN, 10 mM NH_4OH). Every 12th well was combined to create 12 pools. Each pool was lyophilized. *Mass spectrometry*: Peptides (10% per pool) were analyzed by nano LC/MS/MS with a Waters NanoAcquity HPLC system interfaced to a ThermoFisher Fusion Lumos mass spectrometer. Peptides were loaded on a trapping column and eluted over a 75-µm analytical column at 350 nl/min; both columns were packed with Luna C18 resin (Phenomenex). Each high pH RP pool was separated over a 2-h gradient (24 h instrument time total). The mass spectrometer was operated in data-dependent mode, with MS and MS/MS performed in the Orbitrap at 60,000 FWHM resolution and 50,000 FWHM resolution, respectively. A 3-s cycle time was employed for all steps. *Data analysis*: Data were analyzed using MaxQuant v1.6.2.3 (Max Planck) and searched against the combined forward and reverse Swissprot *Homo sapiens* protein database. The database was appended with common background proteins. Search parameters were precursor mass tolerance 7 ppm, product ion mass tolerance 20 ppm, 2 missed cleavages allowed, fully tryptic peptides only, fixed modification of carbamidomethyl cysteine, variable modifications of oxidized methionine and protein N-terminal acetylation. Data were filtered 1% protein and peptide level false discovery rate sand requiring at least one unique peptide per protein. Reporter ion intensities were exported for further analysis.

Untargeted high-resolution LC-HRMS lipidomic analysis
Sample preparation. Metabolic quenching, lysis, and lipid extraction was performed by adding 500 µl ice-cold PBS. Crude mitochondrial samples were homogenized using MP Bio Matrix A tubes

at 60 hz for 1 min; 400 µl uncleared supernatant was transferred to a clean glass tube containing 10 µl LipidSplash deuterated lipid internal standards (Avanti Polar Lipids. Alabaster, AL) and subjected to a Folch extraction. Samples were rested on ice for 10 min before phase separation via centrifugation at 2500 × *g* for 15 min; 700 µl of organic phase was dried to completed under nitrogen gas and resuspended in 1:1 acetonitrile:isopropanol, and 3 µl of sample was subjected to online LC-MS analysis.

LC-HRMS method. Analyses were performed by untargeted LC-HRMS. Briefly, samples were injected via a Thermo Vanquish UHPLC and separated over a reversed-phase Thermo Accucore C-18 column (2.1 × 100 mm, 5 µm particle size) maintained at 55°C. For the 30 min LC gradient, the mobile phase consisted of the following: solvent A (50:50 H_2O:ACN 10 mM ammonium acetate/0.1% acetic acid) and solvent B (90:10 IPA:ACN 10 mM ammonium acetate/0.1% acetic acid). Initial loading condition is 30% B. The gradient was the following: over 2 min, increase to 43%B, continue increasing to 55%B over 0.1 min, continue increasing to 65%B over 10 min, continue increasing to 85%B over 6 min, and finally increasing to 100% over 2 min. Hold at 100% for 5 min, followed by equilibration at 30%B for 5 min. The Thermo IDX tribrid mass spectrometer was operated in both positive and negative ESI mode. A data-dependent MS^2 method was used for scanning in Full MS mode from 200 to 1500 m/z at 120,000 resolution with an AGC target of 5e4 for triggering ms^2 fragmentation using stepped HCD collision energies at 20, 40, and 60% in the orbitrap at 15,000 resolution. Source ionization settings were 3.5 and 2.4 kV spray voltage, respectively, for positive and negative mode. Source gas parameters were 35 sheath gas, 5 auxiliary gas at 300°C, and 1 sweep gas. Calibration was performed prior to analysis using the Pierce FlexMix Ion Calibration Solutions (Thermo Fisher Scientific). Internal standard peak areas were then extracted manually using Quan Browser (Thermo Fisher Xcalibur ver. 2.7), normalized to weight and internal standard peak area, then graphed using GraphPad PRISM (ver. 9.0). Untargeted differential comparisons were performed using LipidSearch 4.2 (Thermo Fisher) to generate a ranked list of significant lipid compounds at the class and species-specific levels.

Statistical analysis

Statistical significances were determined using Prism software (GraphPad Software) as indicated in the figure legends.

REFERENCES

Aaltonen MJ, Friedman JR, Osman C, Salin B, di Rago JP, Nunnari J, Langer T, Tatsuta T (2016). MICOS and phospholipid transfer by Ups2-Mdm35 organize membrane lipid synthesis in mitochondria. J Cell Biol 213, 525–534.

Alkhaja AK, Jans DC, Nikolov M, Vukotic M, Lytovchenko O, Ludewig F, Schliebs W, Riedel D, Urlaub H, Jakobs S, et al. (2012). MINOS1 is a conserved component of mitofilin complexes and required for mitochondrial function and cristae organization. Mol Biol Cell 23, 247–257.

Anderson NS, Haynes CM (2020). Folding the Mitochondrial UPR into the Integrated Stress Response. Trends Cell Biol 30, 428–439.

Baker MJ, Lampe PA, Stojanovski D, Korwitz A, Anand R, Tatsuta T, Langer T (2014). Stress-induced OMA1 activation and autocatalytic turnover regulate OPA1-dependent mitochondrial dynamics. EMBO J 33, 578–593.

Battogtokh G, Choi YS, Kang DS, Park SJ, Shim MS, Huh KM, Cho YY, Lee JY, Lee HS, Kang HC (2018). Mitochondria-targeting drug conjugates for cytotoxic, anti-oxidizing and sensing purposes: current strategies and future perspectives. Acta Pharm Sin B 8, 862–880.

Burman JL, Pickles S, Wang C, Sekine S, Vargas JNS, Zhang Z, Youle AM, Nezich CL, Wu X, Hammer JA, et al. (2017). Mitochondrial fission facilitates the selective mitophagy of protein aggregates. J Cell Biol 216, 3231–3247.

Chojnacka M, Gornicka A, Oeljeklaus S, Warscheid B, Chacinska A (2015). Cox17 s. J Biol Chem 290, 15304–15312.

Cieplik F, Jakubovics NS, Buchalla W, Maisch T, Hellwig E, Al-Ahmad A. (2019). Resistance toward chlorhexidine in oral bacteria - is there cause for concern? Front Microbiol 10, 587.

Cogliati S, Enriquez JA, Scorrano L (2016). Mitochondrial cristae: where beauty meets functionality. Trends Biochem Sci 41, 261–273.

Commander R, Wei C, Sharma A, Mouw JK, Burton LJ, Summerbell E, Mahboubi D, Peterson RJ, Konen J, Zhou W, et al. (2020). Subpopulation targeting of pyruvate dehydrogenase and GLUT1 decouples metabolic heterogeneity during collective cancer cell invasion. Nat Commun 11, 1533.

Dabir DV, Hasson SA, Setoguchi K, Johnson ME, Wongkongkathep P, Douglas CJ, Zimmerman J, Damoiseaux R, Teitell MA, Koehler CM (2013). A small molecule inhibitor of redox-regulated protein translocation into mitochondria. Dev Cell 25, 81–92.

Doughty-Shenton D, Joseph JD, Zhang J, Pagliarini DJ, Kim Y, Lu D, Dixon JE, Casey PJ (2010). Pharmacological targeting of the mitochondrial phosphatase PTPMT1. J Pharmacol Exp Ther 333, 584–592.

Ehses S, Raschke I, Mancuso G, Bernacchia A, Geimer S, Tondera D, Martinou JC, Westermann B, Rugarli EI, Langer T (2009). Regulation of OPA1 processing and mitochondrial fusion by m-AAA protease isoenzymes and OMA1. J Cell Biol 187, 1023–1036.

Fessler E, Eckl EM, Schmitt S, Mancilla IA, Meyer-Bender MF, Hanf M, Philippou-Massier J, Krebs S, Zischka H, Jae LT. (2020). A pathway coordinated by DELE1 relays mitochondrial stress to the cytosol. Nature 579, 433–437.

Formosa LE, Maghool S, Sharpe AJ, Reljic B, Muellner-Wong L, Stroud DA, Ryan MT, Maher MJ (2021). Mitochondrial COA7 is a heme-binding protein involved in the early stages of complex IV assembly. bioRxiv, doi: https://doi.org/10.1101/2021.06.10.447992

Friedman JR, Mourier A, Yamada J, McCaffery JM, Nunnari J (2015). MICOS coordinates with respiratory complexes and lipids to establish mitochondrial inner membrane architecture. eLife 4, e07739.

Guo X, Aviles G, Liu Y, Tian R, Unger BA, Lin YT, Wiita AP, Xu K, Correia MA, Kampmann M (2020). Mitochondrial stress is relayed to the cytosol by an OMA1-DELE1-HRI pathway. Nature 579, 427–432.

Hasson SA, Damoiseaux R, Glavin JD, Dabir DV, Walker SS, Koehler CM (2010). Substrate specificity of the TIM22 mitochondrial import pathway revealed with small molecule inhibitor of protein translocation. Proc Natl Acad Sci USA 107, 9578–9583.

Head B, Griparic L, Amiri M, Gandre-Babbe S, van der Bliek AM. (2009). Inducible proteolytic inactivation of OPA1 mediated by the OMA1 protease in mammalian cells. J Cell Biol 187, 959–966.

Hoppins S, Collins SR, Cassidy-Stone A, Hummel E, Devay RM, Lackner LL, Westermann B, Schuldiner M, Weissman JS, Nunnari J (2011). A mitochondrial-focused genetic interaction map reveals a scaffold-like complex required for inner membrane organization in mitochondria. J Cell Biol 195, 323–340.

Horvath SE, Daum G (2013). Lipids of mitochondria. Prog Lipid Res 52, 590–614.

Igarashi K, Sun J (2006). The heme-Bach1 pathway in the regulation of oxidative stress response and erythroid differentiation. Antioxid Redox Signal 8, 107–118.

Jin SM, Lazarou M, Wang C, Kane LA, Narendra DP, Youle RJ. (2010). Mitochondrial membrane potential regulates PINK1 import and proteolytic destabilization by PARL. J Cell Biol 191, 933–942.

Kenny HA, Lal-Nag M, White EA, Shen M, Chiang CY, Mitra AK, Zhang Y, Curtis M, Schryver EM, Bettis S, et al. (2015). Quantitative high throughput screening using a primary human three-dimensional organotypic culture predicts in vivo efficacy. Nat Commun 6, 6220.

Kondadi AK, Anand R, Hansch S, Urbach J, Zobel T, Wolf DM, Segawa M, Liesa M, Shirihai OS, Weidtkamp-Peters S, et al. (2020). Cristae undergo continuous cycles of membrane remodelling in a MICOS-dependent manner. EMBO Rep 21, e49776.

Korwitz A, Merkwirth C, Richter-Dennerlein R, Troder SE, Sprenger HG, Quiros PM, Lopez-Otin C, Rugarli EI, Langer T (2016). Loss of OMA1 delays neurodegeneration by preventing stress-induced OPA1 processing in mitochondria. J Cell Biol 212, 157–166.

Kozjak-Pavlovic V, Prell F, Thiede B, Gotz M, Wosiek D, Ott C, Rudel T (2014). C1orf163/RESA1 is a novel mitochondrial intermembrane space protein connected to respiratory chain assembly. J Mol Biol 426, 908–920.

Langmaier J, Pizl M, Samec Z, Zalis S (2016). Extreme basicity of biguanide drugs in aqueous solutions: ion transfer voltammetry and DFT calculations. J Phys Chem A 120, 7344–7350.

Lazarou M, Sliter DA, Kane LA, Sarraf SA, Wang C, Burman JL, Sideris DP, Fogel AI, Youle RJ (2015). The ubiquitin kinase PINK1 recruits autophagy receptors to induce mitophagy. Nature 524, 309–314.

Lin TY, Weibel DB (2016). Organization and function of anionic phospholipids in bacteria. Appl Microbiol Biotechnol 100, 4255–4267.

Liu X, Zheng H, Yu WM, Cooper TM, Bunting KD, Qu CK (2015). Maintenance of mouse hematopoietic stem cells ex vivo by reprogramming cellular metabolism. Blood 125, 1562–1565.

Liu YT, Huang X, Nguyen D, Shammas MK, Wu BP, Dombi E, Springer DA, Poulton J, Sekine S, Narendra DP (2020). Loss of CHCHD2 and CHCHD10 activates OMA1 peptidase to disrupt mitochondrial cristae phenocopying patient mutations. Hum Mol Genet 29, 1547–1567.

Matsuda N, Sato S, Shiba K, Okatsu K, Saisho K, Gautier CA, Sou YS, Saiki S, Kawajiri S, Sato F, et al. (2010). PINK1 stabilized by mitochondrial depolarization recruits Parkin to damaged mitochondria and activates latent Parkin for mitophagy. J Cell Biol 189, 211–221.

McDonnell G, Russell AD (1999). Antiseptics and disinfectants: activity, action, and resistance. Clin Microbiol Rev 12, 147–179.

McQuin C, Goodman A, Chernyshev V, Kamentsky L, Cimini BA, Karhohs KW, Doan M, Ding L, Rafelski SM, Thirstrup D, et al. (2018). CellProfiler 3.0: Next-generation image processing for biology. PLoS Biol 16, e2005970.

Merkwirth C, Dargazanli S, Tatsuta T, Geimer S, Lower B, Wunderlich FT, von Kleist-Retzow JC, Waisman A, Westermann B, Langer T (2008). Prohibitins control cell proliferation and apoptosis by regulating OPA1-dependent cristae morphogenesis in mitochondria. Genes Dev 22, 476–488.

Merkwirth C, Martinelli P, Korwitz A, Morbin M, Bronneke HS, Jordan SD, Rugarli EI, Langer T (2012). Loss of prohibitin membrane scaffolds impairs mitochondrial architecture and leads to tau hyperphosphorylation and neurodegeneration. PLoS Genet 8, e1003021.

Michaud M, Gros V, Tardif M, Brugiere S, Ferro M, Prinz WA, Toulmay A, Mathur J, Wozny M, Falconet D, et al. (2016). AtMic60 is involved in plant mitochondria lipid trafficking and is part of a large complex. Curr Biol 26, 627–639.

Mohanraj K, Wasilewski M, Beninca C, Cysewski D, Poznanski J, Sakowska P, Bugajska Z, Deckers M, Dennerlein S, Fernandez-Vizarra E, et al. (2019). Inhibition of proteasome rescues a pathogenic variant of respiratory chain assembly factor COA7. EMBO Mol Med 11, e9561.

Munch C, Harper JW (2016). Mitochondrial unfolded protein response controls matrix pre-RNA processing and translation. Nature 534, 710–713.

Narendra D, Tanaka A, Suen DF, Youle RJ (2008). Parkin is recruited selectively to impaired mitochondria and promotes their autophagy. J Cell Biol 183, 795–803.

Narendra DP, Jin SM, Tanaka A, Suen DF, Gautier CA, Shen J, Cookson MR, Youle RJ (2010). PINK1 is selectively stabilized on impaired mitochondria to activate Parkin. PLoS Biol 8, e1000298.

Nath AK, Ryu JH, Jin YN, Roberts LD, Dejam A, Gerszten RE, Peterson RT (2015). PTPMT1 inhibition lowers glucose through succinate dehydrogenase phosphorylation. Cell Rep 10, 694–701.

Nezich CL, Wang C, Fogel AI, Youle RJ (2015). MiT/TFE transcription factors are activated during mitophagy downstream of Parkin and Atg5. J Cell Biol 210, 435–450.

Nomura K, Imai H, Koumura T, Kobayashi T, Nakagawa Y (2000). Mitochondrial phospholipid hydroperoxide glutathione peroxidase inhibits the release of cytochrome c from mitochondria by suppressing the peroxidation of cardiolipin in hypoglycaemia-induced apoptosis. Biochem J 351, 183–193.

Okatsu K, Oka T, Iguchi M, Imamura K, Kosako H, Tani N, Kimura M, Go E, Koyano F, Funayama M, et al. (2012). PINK1 autophosphorylation upon membrane potential dissipation is essential for Parkin recruitment to damaged mitochondria. Nat Commun 3, 1016.

Osman C, Haag M, Potting C, Rodenfels J, Dip PV, Wieland FT, Brugger B, Westermann B, Langer T (2009a). The genetic interactome of prohibitins: coordinated control of cardiolipin and phosphatidylethanolamine by conserved regulators in mitochondria. J Cell Biol 184, 583–596.

Osman C, Merkwirth C, Langer T (2009b). Prohibitins and the functional compartmentalization of mitochondrial membranes. J Cell Sci 122, 3823–3830.

Quiros PM, Prado MA, Zamboni N, D'Amico D, Williams RW, Finley D, Gygi SP, Auwerx J (2017). Multi-omics analysis identifies ATF4 as a key regulator of the mitochondrial stress response in mammals. J Cell Biol 216, 2027–2045.

Rampelt H, Zerbes RM, van der Laan M, Pfanner N (2017). Role of the mitochondrial contact site and cristae organizing system in membrane architecture and dynamics. Biochim Biophys Acta Mol Cell Res 1864, 737–746.

Richter U, Lahtinen T, Marttinen P, Suomi F, Battersby BJ (2015). Quality control of mitochondrial protein synthesis is required for membrane integrity and cell fitness. J Cell Biol 211, 373–389.

Richter-Dennerlein R, Korwitz A, Haag M, Tatsuta T, Dargazanli S, Baker M, Decker T, Lamkemeyer T, Rugarli EI, Langer T (2014). DNAJC19, a mitochondrial cochaperone associated with cardiomyopathy, forms a complex with prohibitins to regulate cardiolipin remodeling. Cell Metab 20, 158–171.

Rodriguez ME, Azizuddin K, Zhang P, Chiu SM, Lam M, Kenney ME, Burda C, Oleinick NL (2008). Targeting of mitochondria by 10-N-alkyl acridine orange analogues: role of alkyl chain length in determining cellular uptake and localization. Mitochondrion 8, 237–246.

Sanjana NE, Shalem O, Zhang F (2014). Improved vectors and genome-wide libraries for CRISPR screening. Nat Methods 11, 783–784.

Sekine S (2020). PINK1 import regulation at a crossroad of mitochondrial fate: the molecular mechanisms of PINK1 import. J Biochem 167, 217–224.

Sekine S, Kanamaru Y, Koike M, Nishihara A, Okada M, Kinoshita H, Kamiyama M, Maruyama J, Uchiyama Y, Ishihara N, et al. (2012). Rhomboid protease PARL mediates the mitochondrial membrane potential loss-induced cleavage of PGAM5. J Biol Chem 287, 34635–34645.

Sekine S, Wang C, Sideris DP, Bunker E, Zhang Z, Youle RJ (2019). Reciprocal roles of Tom7 and OMA1 during mitochondrial import and activation of PINK1. Mol Cell 73, 1028–1043.e1025.

Shalem O, Sanjana NE, Hartenian E, Shi X, Scott DA, Mikkelson T, Heckl D, Ebert BL, Root DE, Doench JG, et al. (2014). Genome-scale CRISPR-Cas9 knockout screening in human cells. Science 343, 84–87.

Sibrian-Vazquez M, Nesterova IV, Jensen TJ, Vicente MG (2008). Mitochondria targeting by guanidine- and biguanidine-porphyrin photosensitizers. Bioconjug Chem 19, 705–713.

Smith A (2000). Links between cell-surface events involving redox-active copper and gene regulation in the hemopexin heme transport system. Antioxid Redox Signal 2, 157–175.

Steglich G, Neupert W, Langer T (1999). Prohibitins regulate membrane protein degradation by the m-AAA protease in mitochondria. Mol Cell Biol 19, 3435–3442.

Stephan T, Bruser C, Deckers M, Steyer AM, Balzarotti F, Barbot M, Behr TS, Heim G, Hubner W, Ilgen P, et al. (2020). MICOS assembly controls mitochondrial inner membrane remodeling and crista junction redistribution to mediate cristae formation. EMBO J 39, e104105.

Tamura Y, Kawano S, Endo T (2020). Lipid homeostasis in mitochondria. Biol Chem 401, 821–833.

Tatsuta T, Langer T (2017). Intramitochondrial phospholipid trafficking. Biochim Biophys Acta Mol Cell Biol Lipids 1862, 81–89.

Tatsuta T, Model K, Langer T (2005). Formation of membrane-bound ring complexes by prohibitins in mitochondria. Mol Biol Cell 16, 248–259.

Tirrell PS, Nguyen KN, Luby-Phelps K, Friedman JR (2020). MICOS subcomplexes assemble independently on the mitochondrial inner membrane in proximity to ER contact sites. J Cell Biol 219, e202003024.

van der Laan M, Bohnert M, Wiedemann N, Pfanner N (2012). Role of MINOS in mitochondrial membrane architecture and biogenesis. Trends Cell Biol 22, 185–192.

Wai T, Saita S, Nolte H, Muller S, Konig T, Richter-Dennerlein R, Sprenger HG, Madrenas J, Muhlmeister M, Brandt U, et al. (2016). The membrane scaffold SLP2 anchors a proteolytic hub in mitochondria containing PARL and the i-AAA protease YME1L. EMBO Rep 17, 1844–1856.

Wang C, Niederstrasser H, Douglas PM, Lin R, Jaramillo J, Li Y, Oswald NW, Zhou A, McMillan EA, Mendiratta S, et al. (2017). Small-molecule

TFEB pathway agonists that ameliorate metabolic syndrome in mice and extend C. elegans lifespan. Nat Commun 8, 2270.

Weber TA, Koob S, Heide H, Wittig I, Head B, van der Bliek A, Brandt U, Mittelbronn M, Reichert AS (2013). APOOL is a cardiolipin-binding constituent of the Mitofilin/MINOS protein complex determining cristae morphology in mammalian mitochondria. PLoS One 8, e63683.

Wolf DM, Segawa M, Kondadi AK, Anand R, Bailey ST, Reichert AS, van der Bliek AM, Shackelford DB, Liesa M, Shirihai OS (2019). Individual cristae within the same mitochondrion display different membrane potentials and are functionally independent. EMBO J 38, e101056.

Xiao J, Engel JL, Zhang J, Chen MJ, Manning G, Dixon JE (2011). Structural and functional analysis of PTPMT1, a phosphatase required for cardiolipin synthesis. Proc Natl Acad Sci USA 108, 11860–11865.

Xu W, Barrientos T, Andrews NC (2013). Iron and copper in mitochondrial diseases. Cell Metab 17, 319–328.

Yamano K, Youle RJ (2013). PINK1 is degraded through the N-end rule pathway. Autophagy 9, 1758–1769.

Yan C, Gong L, Chen L, Xu M, Abou-Hamdan H, Tang M, Desaubry L, Song Z (2020). PHB2 (prohibitin 2) promotes PINK1-PRKN/Parkin-dependent mitophagy by the PARL-PGAM5-PINK1 axis. Autophagy 16, 419–434.

Youle RJ (2019). Mitochondria-Striking a balance between host and endo-symbiont. Science 365.

Youle RJ, Narendra DP (2011). Mechanisms of mitophagy. Nat Rev Mol Cell Biol 12, 9–14.

Zhang J, Guan Z, Murphy AN, Wiley SE, Perkins GA, Worby CA, Engel JL, Heacock P, Nguyen OK, Wang JH, et al. (2011). Mitochondrial phosphatase PTPMT1 is essential for cardiolipin biosynthesis. Cell Metab 13, 690–700.

Zhang JH, Chung TD, Oldenburg KR (1999). A simple statistical parameter for use in evaluation and validation of high throughput screening assays. J Biomol Screen 4, 67–73.

Zhang K, Li H, Song Z (2014). Membrane depolarization activates the mitochondrial protease OMA1 by stimulating self-cleavage. EMBO Rep 15, 576–585.